PUBLISHED VERSION (DOI): 10.1016/j.autcon.2019.04.021

Non-destructive means and methods for structural diagnosis of masonry arch bridges

Luis Javier Sánchez-Aparicio[1*], Álvaro Bautista-De Castro[1], Borja Conde[2], Pedro Carrasco[1], Luís F. Ramos[3]

[1] Department of Cartographic and Land Engineering. University of Salamanca, High Polytechnic School of Ávila, Hornos Caleros, 50, 05003, Ávila (Spain). L.J.S.A (luisj@usal.es), A.B.C (alvarobautistadecastro@usal.es), P.C.G (retep81@usal.es)

[2] University of Vigo, School of Industrial Engineering, Department of Engineering Materials, Applied Mechanics and Construction, Vigo, Spain. B.C.C. (bconde@uvigo.es)

[3] ISISE, Department of Civil Engineering, University of Minho, Campus de Azurém, 4800-058 Guimarães, Portugal. L.F.R. (lramos@civil.uminho.pt)

*Corresponding author: Tlf.: +34 920353500; Fax: +34 920353501;

e-mail address: luisj@usal.es

Abstract

Within the precepts defended by the International Charter of Kraków, this paper aims at presenting a fully non-destructive multidisciplinary approach able to characterize masonry bridges at three different levels: i) geometrical level; ii) material level and; iii) structural level. To this end, this approach integrates the terrestrial laser scanner, the sonic and impact-echo methods, the ground penetrating radar and the multichannel analysis of surface waves. All these data are combined with reverse engineering procedures, allowing the creation of suitable as-built CAD models for advanced numerical simulations. Then, these numerical models are contrasted and updated through the data provided by the ambient vibration tests. To validate the methodology proposed in this paper, the Roman bridge of Avila was used as study case. This bridge shows a complex mixture of constructive techniques (masonry, cohesive material, *Opus Caementicium* and reinforced concrete). Thus, the numerical model was considered for performing predictive structural analysis.

Keywords: Historical constructions; Masonry arch bridge; Non-destructive testing; Terrestrial laser scanner; Sonic testing; Multichannel analysis of surface waves; Ground Penetrating Radar; Ambient vibration tests; Finite Element Method; Non-linear analysis.

1 Introduction

Among the wide variety of constructive typologies that make up our historical legacy, masonry arch bridges have been placed as one of the most important elements through history, being still an essential part within the current communication networks. Many of these ancient constructions are at present supporting potentially destructive conditions due to new traffic loads, large vibrations, foundation settlements, extreme natural events

(e.g., earthquakes, river overflows or floods) and environmental agents (e.g., the presence of high levels of moisture or melting salts) [1]. The combination of these effects progressively induces the deterioration of the materials and the development of damage phenomena expressed in the form of cracks or permanent deformations [2-4]. It is for that reason that is necessary to carry out a comprehensive structural diagnosis in order to know the current and the future structural condition of these types of infrastructures and consequently, designing proper conservation or restoration actions.

Among the different numerical modeling strategies proposed so far to evaluate masonry arch bridges mechanical behavior, from the Limit Analysis theory or the Discrete Element Method, the Finite Element Method [4] has been placed as one of the most powerful. This approach has allowed successfully simulating masonry bridges under different casuistic such as settlements [2], pier scours [5], seismic actions and live loads [6-10], being possible to replicate the damages that appears along the history of the construction [2, 11].

Despite this potentiality, one of the major drawbacks of this computational modeling approach is that it requires extensive knowledge of the physical and mechanical properties of the materials present on the structure, and thus the need of using multidisciplinary approaches to collect the required input data [12]. Under this framework, several studies in the past have been focused on the development of multidisciplinary strategies targeted to characterize masonry arch bridges at different levels [8, 13-15]: i) at geometrical level; ii) at material level and; iii) at the structural system level.

Concerning the first level, i.e., the geometry, this type of constructions is typically characterized by its high complexity in terms of size, location, and inner composition. These challenges place the terrestrial laser scanner and the digital cameras by means of the photogrammetric method, as the most used sensors to characterize the external envelope of this typology of bridges [13, 15-21]. The product obtained from these geomatic sensors, the so-called point cloud, is then employed for the creation of CAD model suitable for structural analysis by means of one of the following approaches [22]: i) creation of CAD models based on sections and individual measurements coming from the point cloud obtained [8, 11, 17, 21]; ii) meshing of the point cloud and creation of the CAD model based on the mesh [22-24] and; iii) creation of non-uniform rational b-splines from the point cloud [24, 25]. Additionally, it is possible to find in the literature procedures able to exploit the concept of the point cloud voxelization such as the Cloud2FEM procedure proposed by Castellazzi et al. [11, 26, 27]. Even though these procedures are able to generated a numerical mesh from the point cloud in a semi-automatic way. However, these methods require a point cloud with few holes and tend to generate numerical meshes with a large number of elements. Apart of this, the presence of deformations can be hardly captured by means of these methods. In contrast to these strategies, it is possible to find approaches based on the last advances in reverse engineering. These approaches exploit use methods such as the extrusion of surfaces or b-splines to represent CAD models on which is possible to control its level of detail [12, 28]. Complementary to these techniques, the ground penetrating radar method has also been extensively used in order to characterize the inner composition of masonry arch bridges, such as the thickness of its barrel vaults or the layering of the infill materials [6, 13, 19, 20, 29].

Regarding the second level, the characterization of the constituent materials, masonry arch bridges present two main components: i) the masonry and; ii) the infill. On the one hand, the masonry has been used to build the main load-bearing parts of the bridge, such as the barrel vaults, spandrel walls and piers as well as other secondary elements such as

buttress or cutwaters. Masonry mechanical properties can be characterized resorting to laboratory tests (e.g., compression tests) or even in-situ tests through the use of the flat-jack tests. On the one hand, the first approach is very time-consuming since it requires the confection of several masonry samples. On the other hand, the flat-jack tests are invasive, requiring the preparation of a slot on which is inserted a thin envelope-like bladder that is pressurized with a fluid. Thus, as an alternative, the sonic testing approach has recently emerged as a suitable non-destructive testing technique aimed to characterize the physical and mechanical properties of masonry [19, 30]. On the other hand, the infill material helps by dispersing the loads coming from the road surface up to the vaults and in its stabilization by providing additional lateral stiffness. The contribution of the infill material to the overall bridge strength is generally high, being an important aspect that should be taken into account in the structural assessment procedure, as it has been highlighted in previous research works [8, 10]. However, the accurate characterization of the physical and mechanical parameters of infill materials poses a great challenge nowadays, requiring the use of invasive techniques to extract samples [31], or even the use of other invasive methods such as the Ménard Pressuremeter tests to locally characterize the infill properties [6, 32].

Finally, with regards to the third level, i.e., the characterization of the structural system at the global level, several authors have considered the ambient vibration tests as the most suitable technique for evaluating the global response of this type of structures [10, 19, 32]. This approach allows obtaining the dynamic response of the structure, namely its natural frequencies and mode shapes, under operational conditions. These dynamic properties can be posteriorly considered within a constrained optimization framework whose main goal is obtaining a set of input values for the Finite Element model of the structure (e.g., Young´s Modulus of the masonry or infill) so that model outcomes best fit the experimentally obtained response of the structure; thus better representing its current mechanical behavior in operational conditions [8, 19, 32].

According to the above mentioned, the success of any numerical simulation, and hence the ability to emit an accurate structural diagnosis, strongly depends on the knowledge of the different constructive elements and the physical and mechanical properties of the materials in which are executed. Under this basis, and inside the framework of the modern restoration theory based on the precepts defended by the International Charter of Kraków [33], this paper proposes a multidisciplinary approach, fully based on non-destructive methods, aimed to generate high-fidelity numerical models. To this end, the approach combines well-known methods in the structural evaluation of masonry bridges such as the terrestrial laser scanner or the ground penetrating radar [20, 21, 34] with other procedures able to overcome part of the main limitations of the current multidisciplinary approaches. Among these limitations stand out: i) the capacity of charactering, in-situ and from a non-destructive point of view, part of the mechanical properties of the masonry and the infill; ii) the use of additional tests able to supplement the information provided by the ground penetrating radar and; iii) a method, based on the latest advances in reverse engineering, able to generate as-built CAD models that reproduces the current deformed state of the bridge.

To validate proposed non-destructive methodology in the differeent levels previously highlighed, the roman bridge of Avila (Castile and León, Spain) is used as a case study. This bridge was initially erected during the age of Trajan to connect the *Decumanus Maximus* of the city with its riverside. However, the presence of anthropic and environmental agents has promoted on the bridge intense changes, currently showing a mixture of constructive systems (roman, medieval and modern) and materials (stone and concrete solutions). According to this, the paper is structured as follows: after this initial

142 introduction, section 2 briefly describes the masonry arch bridge used to validate the
143 multidisciplinary approach. Section 3 exposes the experimental campaign carried out and
144 the obtained results. Section 4 presents the method proposed to generate an accurate
145 numerical simulation of the bridge. Section 5 evaluates the accuracy of the developed
146 model by comparing simulation outcomes with the experimentally obtained dynamic
147 behavior of the bridge. Section 6 provides and discusses the results of the safety
148 evaluation of the bridge, and finally, in section 7 the conclusions are drawn.
149

150 # 2 The Roman bridge over the Adaja river

151 ## 2.1 Historical background

152 The Roman bridge over the Adaja river is located on the road of Extremadura in the Avila
153 city, Spain, concretely in the western part of its Mediaeval Wall (Figure 1). Its origin can
154 be attributed to the Roman epoch, presumably during the Trajan period (98-117 A.C.)
155 due to its similarity, in terms of constructive techniques and design, with other roman
156 bridges erected in the same epoch, such as the Alcantara or the Bibey bridges [35]. The
157 construction of this infrastructure was motivated by the necessity of communicating the
158 *Decumanus Maximus* of the roman city *Abula* with its riverside.
159 In the Mediaeval age, probably during the Muslim invasion of the Iberian Peninsula in
160 the year 711 A.C., the upper part of the bridge was demolished with the purpose of
161 isolating the city. From this demolition, the piers, the cutwaters and the beginnings of
162 some of the vaults have remained intact [35]. During the XIth century, the spandrel walls
163 and the missing parts of the vaults were restored with ochre granite coming from the
164 nearby quarry of "La Colilla". This type of granite was the most used in Avila during the
165 Mediaeval age. However, due to the premature erosion that this kind of material suffers,
166 periodic restoration works were carried out on the bridge, being highlighted the
167 restoration actions carried out in the XIIIth century, in which the parapets were replaced
168 with grey granite masonry (Figure 1).
169

a) b)

170

171 **Figure 1.** General view of the bridge: a) upstream and; b) downstream.
172

173 Between 1788 and 1900 several industrial buildings were annexed to the east part of the
174 bridge (Figure 2). Later, these constructions were demolished around 1996 due to its
175 deficient state of conservation, especially after the fire that took place in 1984 [36]. After
176 the demolition of these buildings, the upstream right side of the bridge was covered with
177 natural soil in order to restore the urban environment (Figure 2b).
178

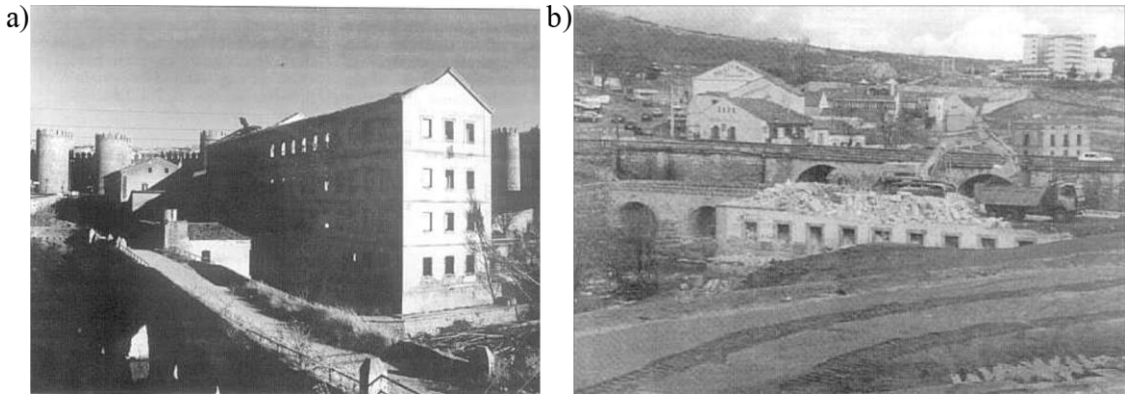

Figure 2. Industrial buildings annexed to the upstream right side of the bridge [36]: a) view from the downstream and; b) image captured during the demolition of these buildings.

More recently, on 21 August 1995, a heavy rainfall damaged the bridge. The damage was promoted by the increase of the infill pressures due to its saturation, partially collapsing the upstream spandrel wall (Figure 3a). This collapse together with the overall deficient state of conservation of the bridge determined the necessity of undertaking major restoration works. These works were carried out during that year, repairing the right side, the left pier of the major vault as well as the central voussoirs of all the minor barrel vaults (Figure 3b). Additionally, the bridge´s deck was completely reconstructed, adding a weather-tightening concrete slab of 15 cm with non-structural steel bars and a granite cobblestone pavement (Figure 3**¡Error! No se encuentra el origen de la referencia.**c and d).

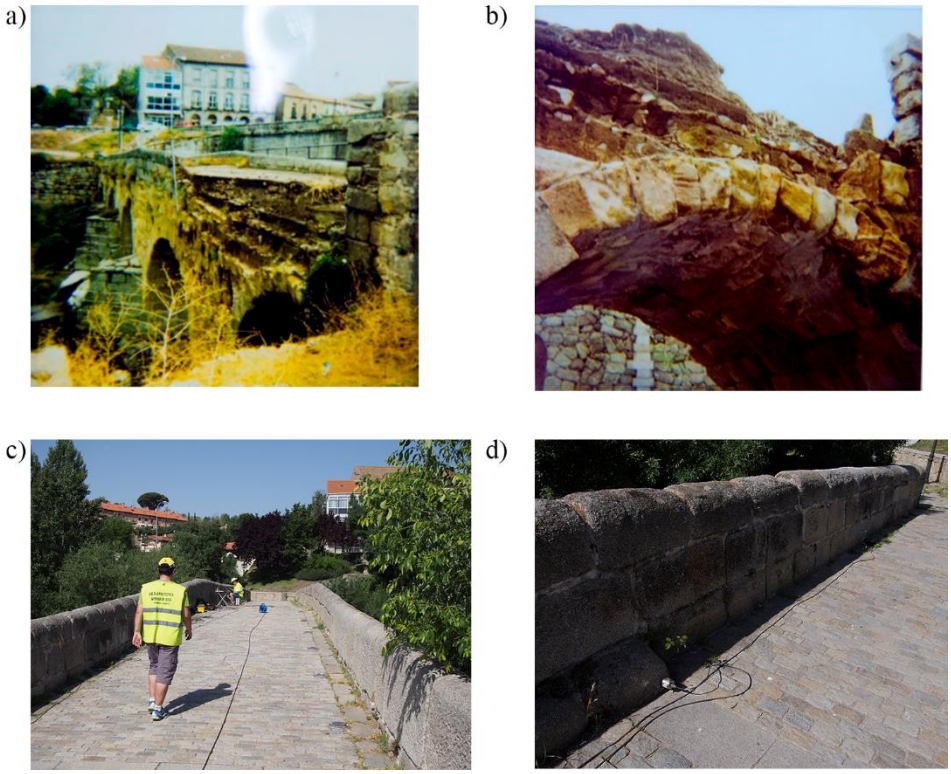

Figure 3. State of conservation before the urgent restoration works carried out in 1995: a) general view of the east spandrel wall after the waterspout; b) state of conservation of the east barrel vault on which is possible to observe heavy material losses (in some sections around the 30% of the original thickness) [37] and; c) and d) details of the granite cobblestone pavement added in 1995. Source: Memoria valorada para la actuación urgente en el Puente romano sobre el Río Adaja (Obras municipales 80/6).

2.2 Constructive description of the bridge

The bridge has a total length of approximately 60.00 m and a total width of 4.14 m, presenting five vaults along its trace These vaults have a rise/span ratio near to 0.50 (Figure 4) (Table 1). Viewing the bridge from the upstream side and from West to East (from the road of Extremadura to the Mediaeval Wall), the barrel vaults 1/2/3/5 show an average span of 6.18 m. In turn, the barrel vault 4 shows higher dimensions with a span of 9.20 m (Figure 4d). The most relevant geometrical features are shown in Table 1.

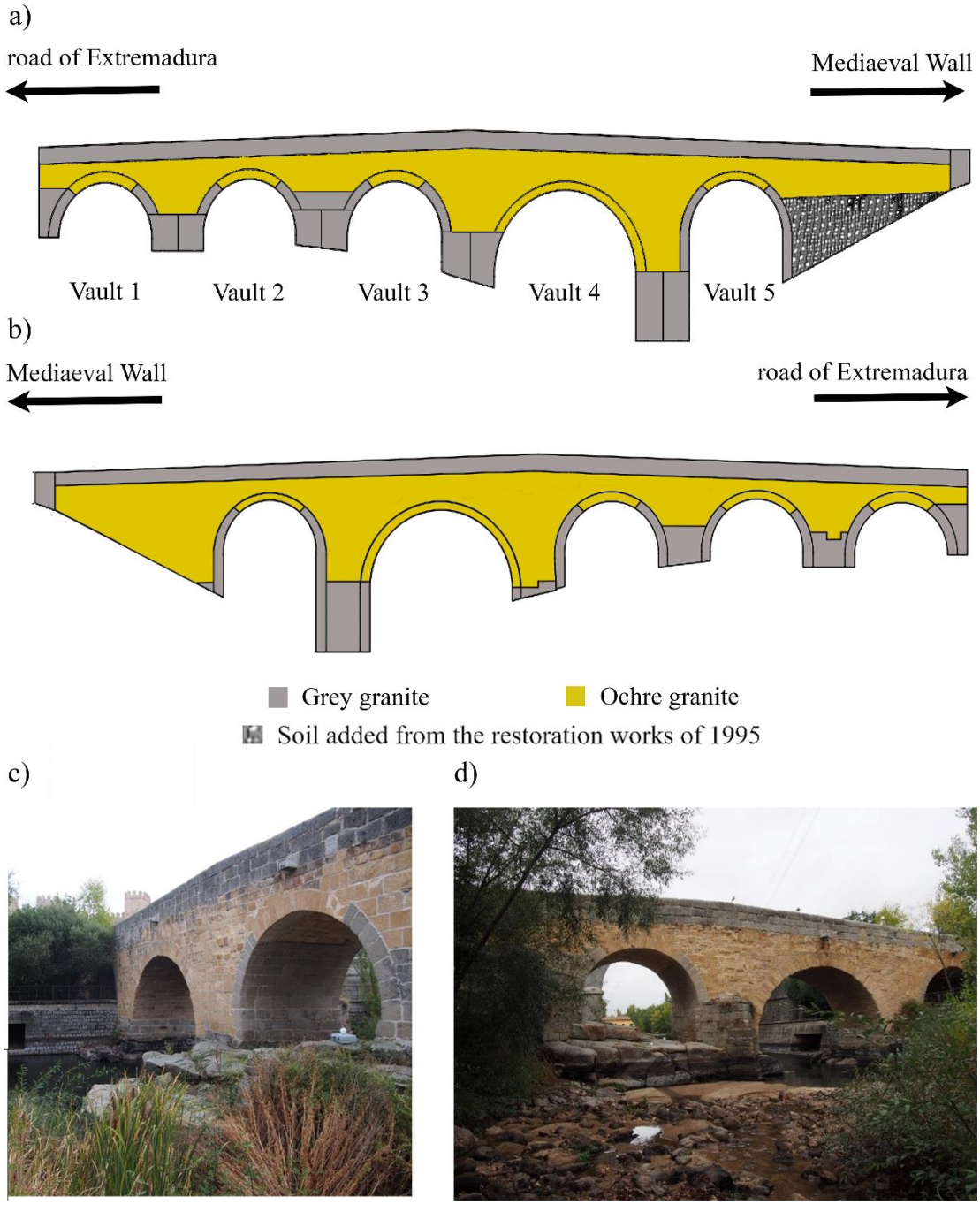

Figure 4. Historical bridge over the Adaja river: a) downstream elevation; b) upstream elevation; c) general view of the upstream side and; d) general view of the downstream side.

Table 1. Geometrical features of the bridge barrel vaults.

Arch	Span (m)	Rise (m)	Rise/Span ratio	Thickness (m)
1 (West)	6.17	3.04	0.49	0.55
2	6.19	3.03	0.49	0.54
3	6.19	3.03	0.49	0.53
4	9.20	4.86	0.53	0.85
5 (East)	6.15	3.05	0.50	0.55

Moreover, this bridge was built over a narrowing of the waterway produced by a rock formation of granite which was used as foundation for the piers of the bridge (Figure 4). These piers are of rectangular shape with an average height of 3.50 m and an average width of 4.66 m, thereby presenting an average pier slenderness (pier height-pier width ratio) of 1.33. To all the piers are attached, in the upstream side, triangular cross-section cutwaters (Figure 4d). These cutwaters have an average height of 2.58 m and an average width of 2.11 m.

Apart from the geometrical features of the barrel vaults, piers and cutwaters, one of the most salient features of this historical bridge is the presence of two types of masonry (Figure 4). On the one hand, a grey granite masonry coming, at the exception of the parapets erected during the medieval period, from the Roman period. This masonry is placed in the lower part of the bridge as well as in all bridge´s cutwaters and it is made up by regular masonry blocks. On the other hand, the upper part of the spandrel walls and the barrel vaults is made up by a regular ochre granite masonry with mortar joints (Figure 4c) (Figure 4d).

Concerning the infill of the bridge, the archaeological samples taken in 1995 revealed the presence of two infill layers: i) a roman concrete with large aggregate size (*Opus Caementicium*) from the foundation until approximately 2/3 of the rise of the vaults and; ii) a compacted cohesive infill with inclusions of large aggregates from the 2/3 of the rise of the vaults until the deck. Over this layer is placed a concrete slab with a total thickness of 0.15 m and a grey granite cobblestone pavement made up by stone blocks whose dimensions are 0.10 x 0.20 x 0.10 m. These stone blocks are with cement mortar (**¡Error! No se encuentra el origen de la referencia.**3c and d). Concerning the parapets, they have an average thickness of approximately 0.38 m and an average height of 1.36 m.

2.3 Analysis of the indicators of damage

Before performing the in-situ non-destructive tests, a damage mapping was carried out with the aim of assessing the current state of conservation of the bridge. This procedure resulted in the following visual indicators of alteration (Figure 5) (Figure 6): i) material losses; ii) deformations; iii) salt crusts; iv) biological colonization; v) moisture; and vi) graffiti.

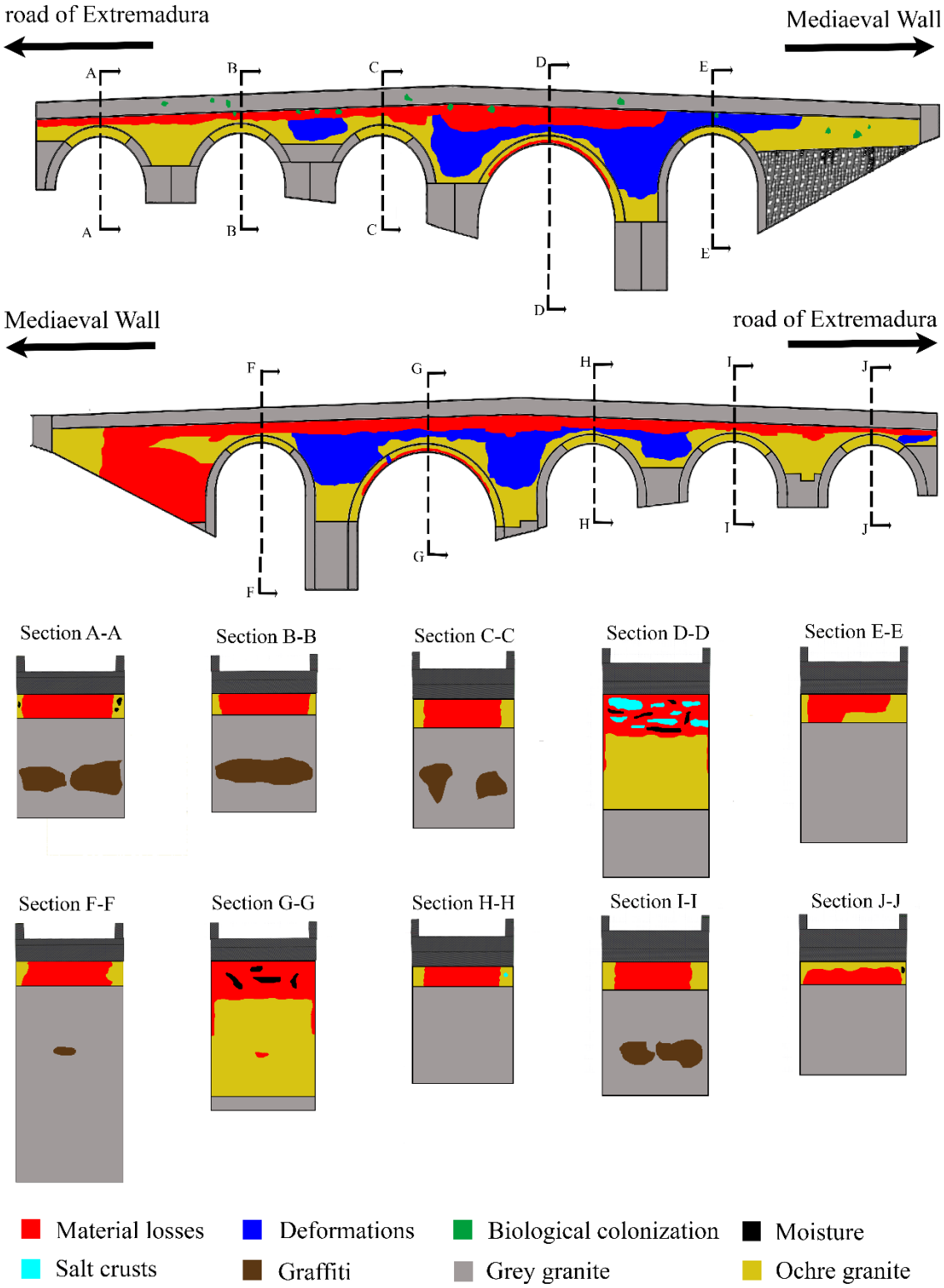

Figure 5. Damage mapping obtained from the visual inspection performed according to the damage indicators defined within the framework of the European research project HeritageCARE [38].

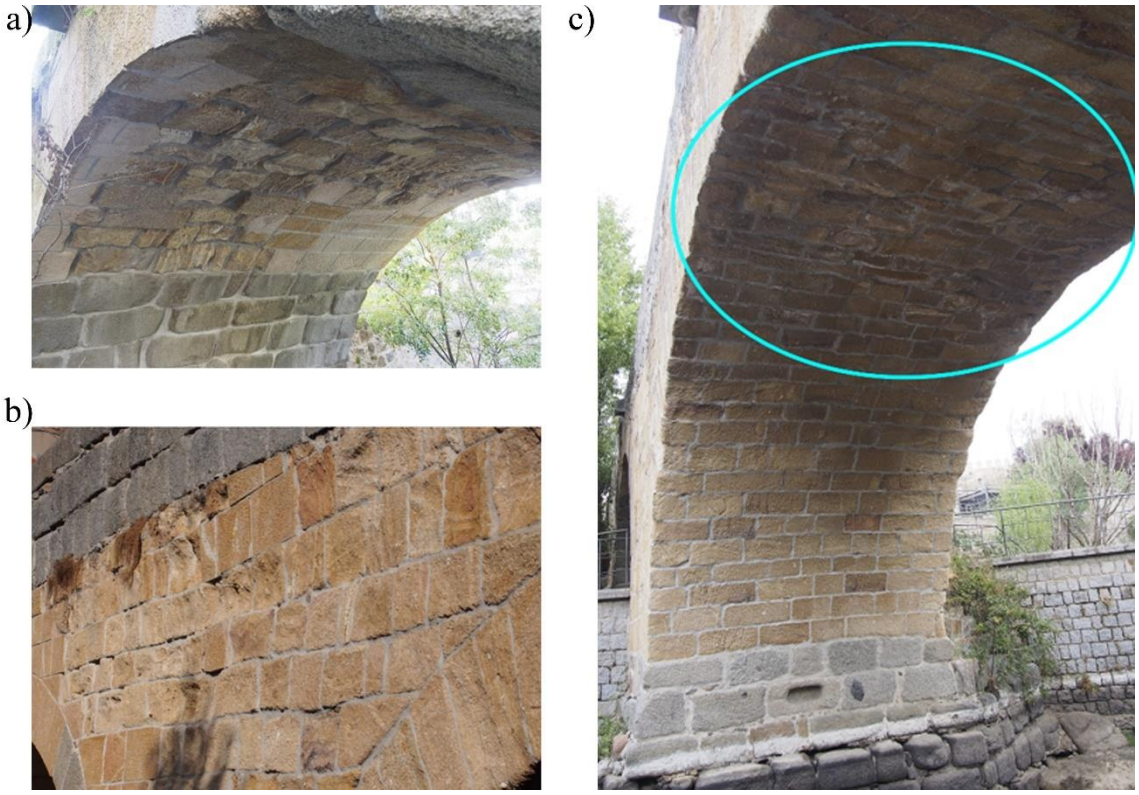

Figure 6. Detail of the bridge´s material losses promoted by the aggressiveness of the environment and the cement mortar used to restore the masonry: a) keystone of the vault 5; b) upstream spandrel wall between the vault 3 and 4 and; c) presence of white crusts on the main barrel vault keystone.

It is worth mentioning the material losses observed on the barrel vaults (Figure 6a) and the spandrel walls (Figure 6b). These pathologies are mainly attributed to the high porosity and low frost resistance of the ochre granite [39], which in combination with the environment and the mechanical and chemical behavior of the cement mortar are promoting material losses. This damage reduces the effective resistance section of the main load-bearing elements of the bridge. Also, it was possible to observe out-of-plane deformations in the upper part of the spandrel walls (Figure 5).

3 Experimental program: geometrical, material and dynamical characterization of the bridge

Considering the necessity of knowing all the structural components of the bridge, from both a geometrical and a mechanical point of view, the following multidisciplinary methodology was adopted (Figure 7).

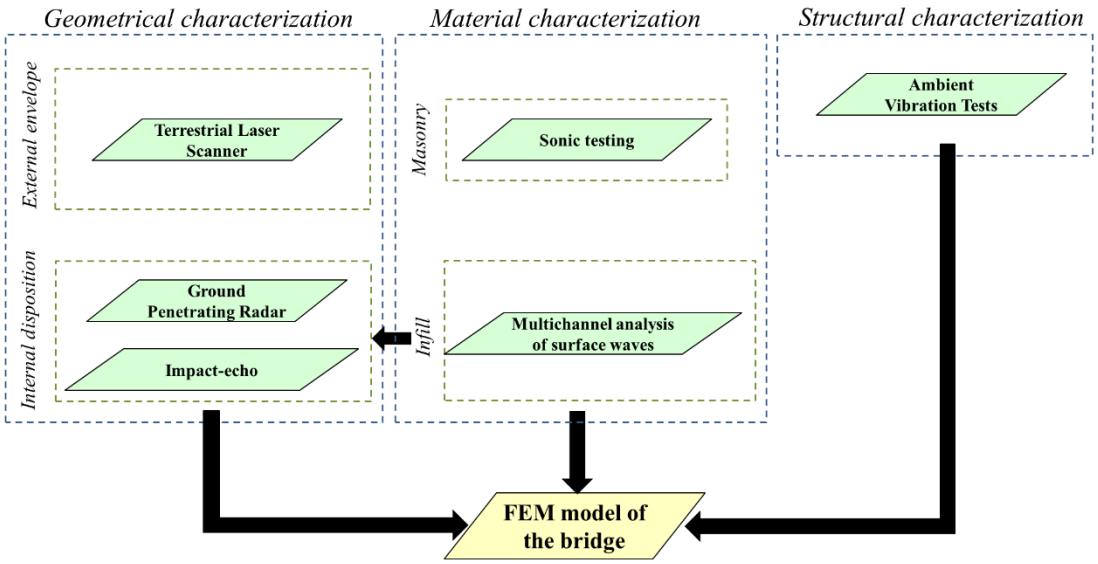

Figure 7. The multidisciplinary methodology employed for the development of an advanced numerical simulation of the bridge.

For the characterization of the external envelop of the bridge it was used the terrestrial laser scanner (TLS). Since this sensor is only able to capture the external geometry of the construction, the ground penetrating radar (GPR), the impact-echo method (IE) and the multichannel analysis of surface waves (MASW) were used. In this case the GPR and the IE method are used to characterize the thicknesses of the spandrel walls and vaults. On the other hand, the MASW method is used to characterize the inner distribution of the infill. All these information is later combined and used to create an as-built CAD model of the bridge by means of reverse engineering procedures.

From the material point of view, the proposed methodology uses the sonic testing for the characterization of the elastic properties of the masonry components. Meanwhile, the MASW method is used to characterize the Young Modulus as well as the density of the infill layers.

Finally, it is proposed the use of the Ambient Vibration Tests with the aim of validating the numerical simulation arose from the previous tests. Result of this combination of tests and procedures it was possible to generate an accurate advance numerical simulation of the construction.

3.1 Geometrical characterization of the bridge

3.1.1 Terrestrial laser scanner survey

Due to the difficulty for accessing to some parts of the bridge, as well as the complexity of its geometry, the use of the terrestrial laser scanning technology was the best solution given its portability, accuracy and working range [12, 40]. Accordingly, the Faro Focus 3D 120 equipment was used to characterize the geometrical envelope of the bridge (Figure 8). This lightweight laser scanner is able to capture 122,000 to 976,000 points per second with a nominal accuracy of 2mm at 25 m.

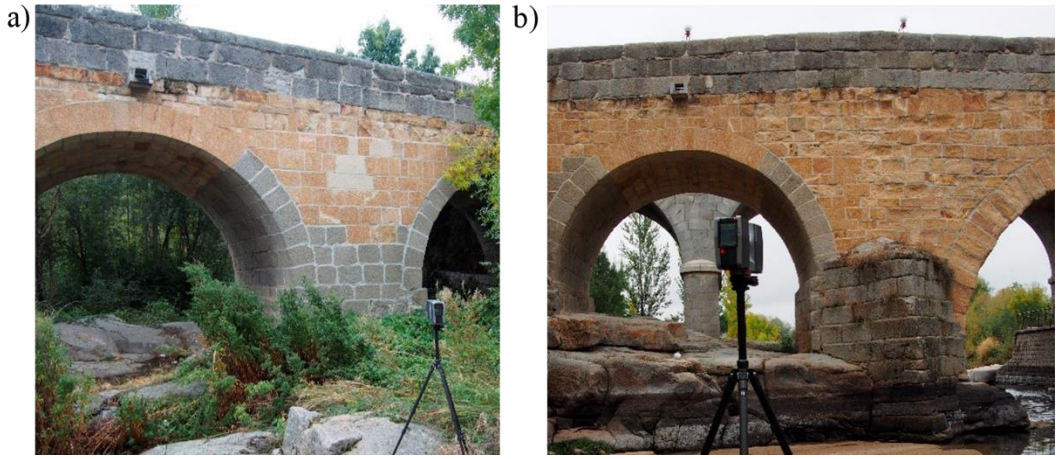

Figure 8. TLS data acquisition: a) Faro Focus 3D and; b) detail of the registration spheres used to align the different scan stations.

Complementary to this sensor, several registration spheres, with two different diameters (200 mm and 145 mm), were used to perform an automatic alignment between the different scan stations. To this end, the target-based procedure defined by Bienert et al. [41] was used.

As a result, a total of sixteen scans were required in order to record the whole bridge structure: i) ten scan stations to capture the downstream part of the bridge and; ii) six scan stations to represent its upper part, obtaining an alignment error of 0.005 ± 0.003 m. The huge amount of data captured was then decimated by applying a density filter with a threshold of 0.01 m. Therefore, an optimized 3D digitalization of the bridge made up by 15,631,250 points (representing the 32% of the total points captured during the experimental campaign) was finally obtained (Figure 9).

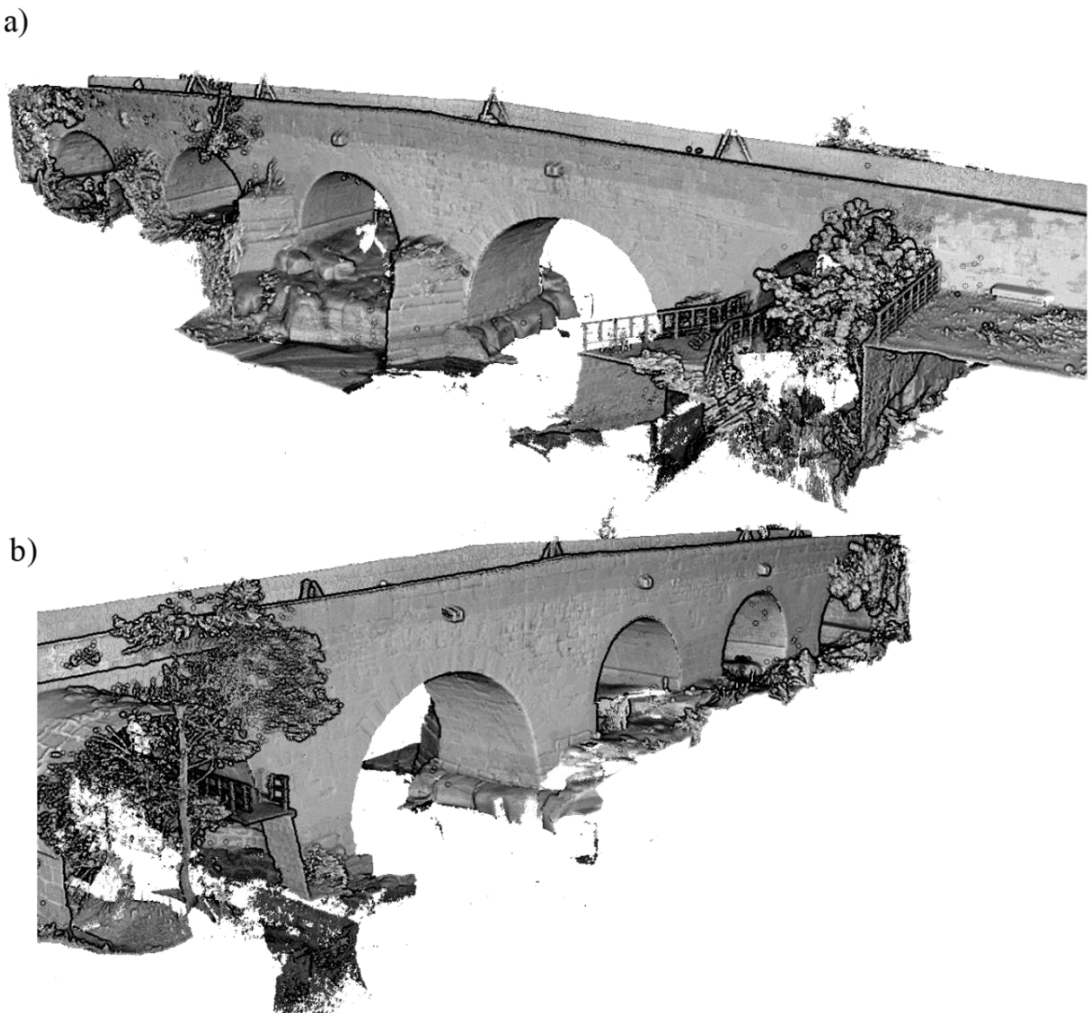

Figure 9. General view of the bridge´s point cloud obtained by the TLS: a) upstream side and; b) downstream side.

3.1.2 Ground penetrating radar survey

Complementary to the TLS survey, the ground penetrating radar (GPR) method was used with the purpose of obtaining the inner structure of the bridge. To this end, the X3M® GPR system from MALA Geoscience was used, performing a total of five radargrams (Figure 10): i) two horizontal profiles along the longitudinal axis of the bridge, with a central frequency of 250 MHz and a total time window of 30 ns and; ii) three profiles in the vertical direction with a central frequency of 800 MHz and a total time window of 100 ns. To scale the profiles, several marks were used during the data acquisition coinciding with the start and end points of each radargram.

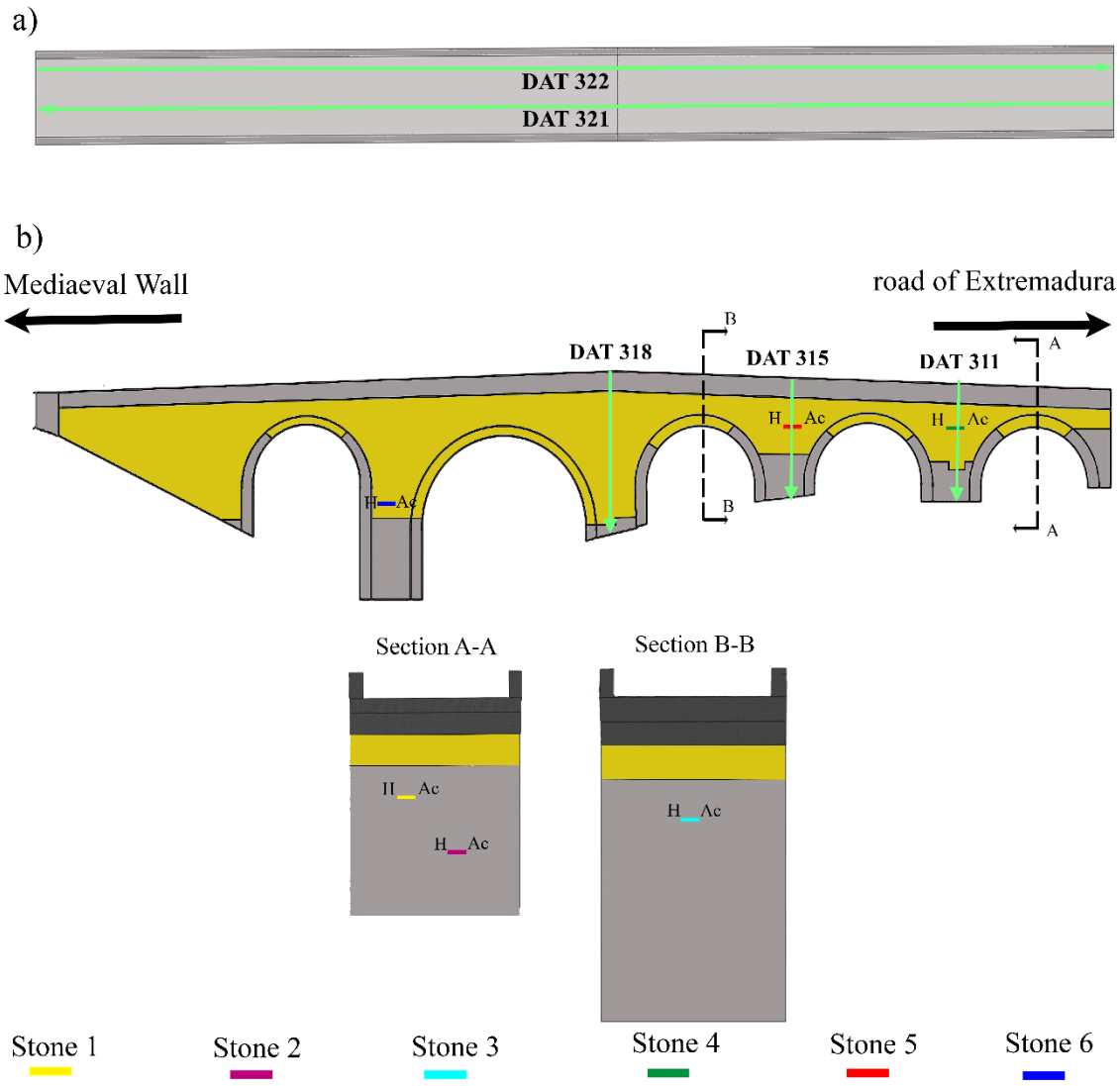

Figure 10. Positions of the GPR, indirect and impact-echo tests carried out on the bridge: a) plant view and; b) downstream elevation. *H* indicates the position of the hammer and *Ac* indicates the position of the transducer during the indirect sonic tests.

On the one hand, the vertical GPR profiles allowed identifying the cross-section of the bridge made up by (Figure 11): i) a granite cobblestone layer with 10.00 cm thickness; ii) a concrete slab with 15.00 cm thickness; iii) a first infill layer from the concrete slab to the 2/3 of the rise of the vaults (Mediaeval infill); iv) a second infill layer from the 2/3 of the rise of the vaults until the foundation (Roman infill) and; v) a masonry foundation. These results were consistent with those obtained during the multichannel analysis of surface waves test (Section 3.2.2) as well as with the archeological samples (Section 2.2). Additionally, it was possible to estimate the thickness of the spandrel walls, with an average value of 0.45 m (Figure 11).

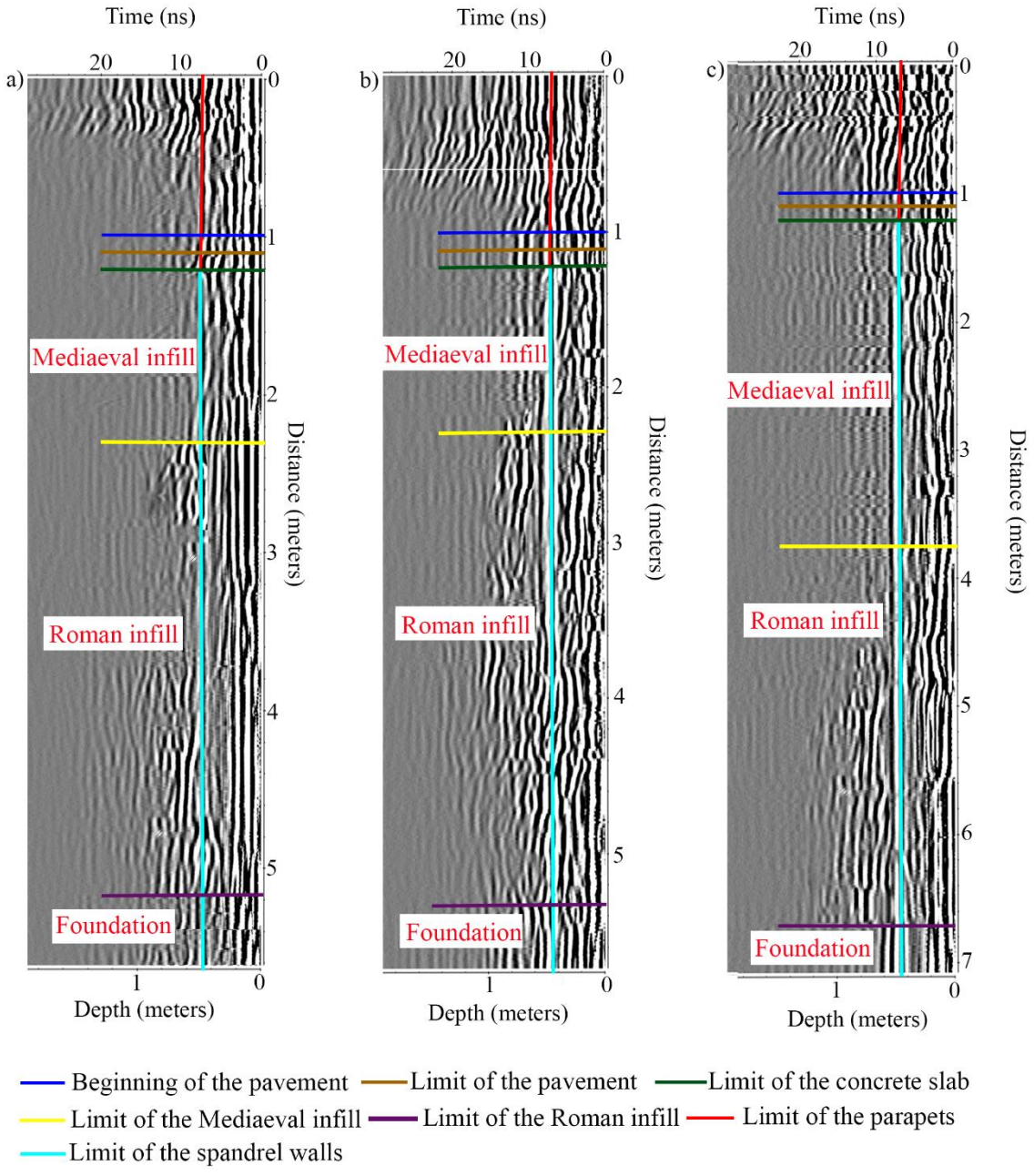

340

341 **Figure 11.** Results obtained from the vertical GPR profiles: a) radargram DAT-31; b) radargram DAT-315
342 and; c) radargram DAT-318.

343

344 On the other hand, the horizontal radargrams were characterized by the presence of a
345 continuous reflection due to the presence of a steel bars within on the bridge´s deck. These
346 bars were used to avoid the presence of cracks due to the retraction of the concrete, not
347 having influence from the structural point of view during the restoration works carried
348 out in 1995. Thus, it was not possible to identify the infill distribution of the bridge
349 (Figure 12). Furthermore, it was possible to observe the presence of expansion joints
350 equally spaced at 6.00m along the concrete slab (Figure 12).

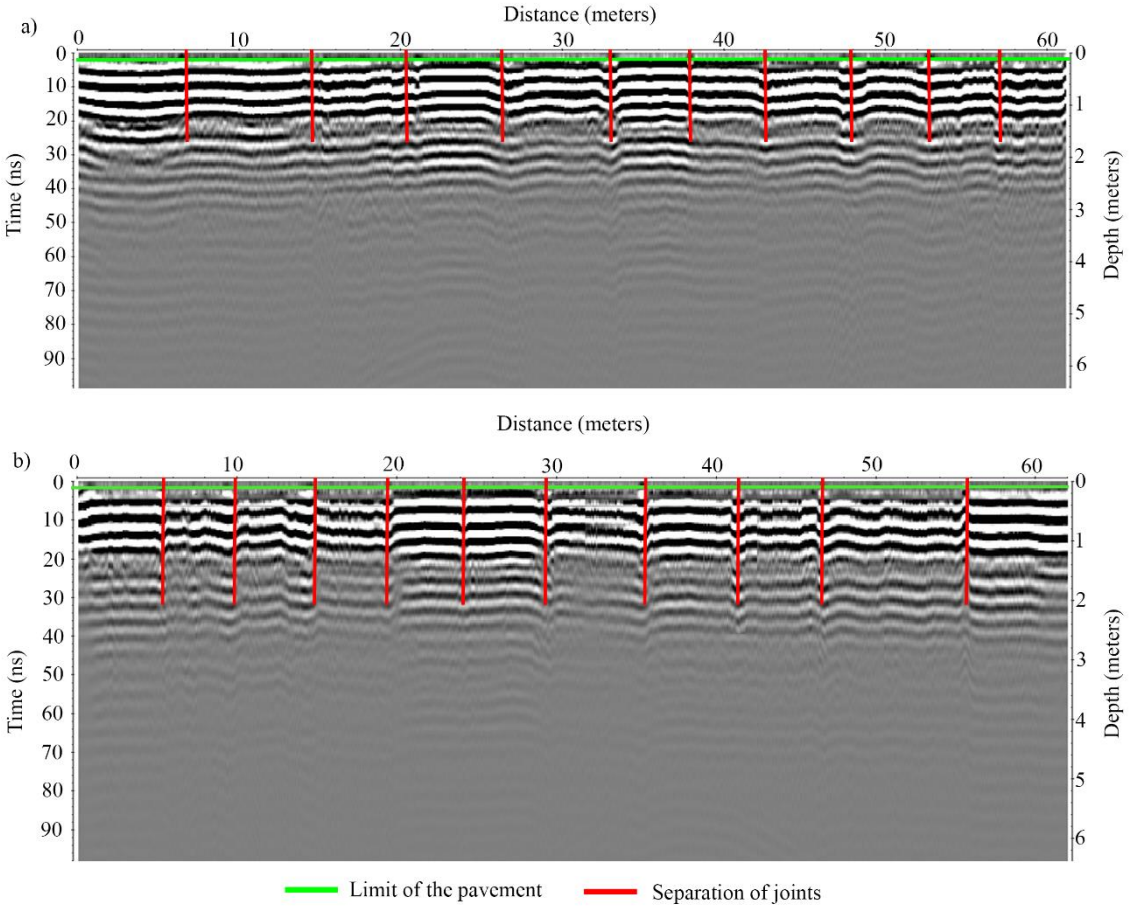

Figure 12. Results obtained from the horizontal GPR profiles: a) radargram DAT-321 and; b) radargram DAT-322.

3.1.3 Impact-echo tests

The impact-echo method was used to characterize the thickness of the masonry elements (spandrel walls and barrel vaults) and verifying the average thickness coming from the vertical profiles obtained from the GPR survey (Figure 11). To perform these impact-echo tests it was used an equipment composed by the following elements: i) an instrumental hammer; ii) a data acquisition unit of 24 bit of resolution with a maximum sampling rate of 100 kHz and; iii) a transducer (piezoelectric accelerometer) with a sensitivity of 10 V/g, range of ± 0.5 g and 8 μg of broadband resolution. It is worth mentioning that the instrumental hammer as well as the transducer were placed in the same position, making possible to establish the starting and the ending point in the same location [42]. The excitation recorded by the transducer was then processed allowing to obtain the frequency spectrum through the use of the Fast Fourier Transform (FFT) [42]. The peaks detected by the FFT indicates the presence of internal heterogeneities which could be attributed to the interface between materials, in this case, masonry-infill.
Consequently, a total of six impact-echo tests were carried out on the bridge (Figure 10b): i) three on the barrel vaults (stone 1 to stone 3) and; ii) three on the spandrel walls (stone 4 to stone 6). To extract the depth of the interface masonry-infill, the following equation was applied (Eq. 1).

$$V_p = 2df \quad (1)$$

where V_p is the P-wave velocity in m/s of the stone block and d is the distance in meters from the receptor to a point with a peak frequency f in Hz.

In order to obtain the velocity of propagation of the P-waves (primary waves), several indirect sonic tests were carried out in the same position than the impact-echo tests. In this case, the hammer was placed at 0.50 m with respect to the transducer (Figure 10b). As expected, the propagation speeds obtained in the ochre granite were lower than the propagation speeds in the grey granite (11.82% lower). This difference can be attributed to the distinct nature of each granite. While the grey specimen can be considered as an unaltered granite, the ochre granite is a silicified facie with more internal discontinuities [39].

Table 2. Propagation velocities obtained during the experimental campaign in each type of granite.

Sample		Propagation speed			
		V_p (m/s)	Cov (%)	V_r (m/s)	Cov (%)
Grey granite	Stone 1	1282.60	1.61	679.78	1.57
	Stone 2	1297.80	1.53	687.73	1.20
	Stone 3	1286.40	1.38	681.79	1.60
Ochre granite	Stone 4	1137.44	1.33	602.84	1.29
	Stone 5	1138.46	1.97	603.38	1.40
	Stone 6	1133.55	1.02	600.78	1.59

The results of the impact-echo tests yielded an average thickness of 0.57 m in the barrel vaults and an average thickness of 0.47 m in the spandrel walls, being the thickness obtained in the spandrel walls consistent with the data provided by the vertical GPR profiles (Figure 11) (Table 3).

Table 3. Results obtained from the impact-echo tests and comparison of the thicknesses data with their counterparts obtained from the vertical GPR profiles. In brackets the covariance, in %, of the frequencies obtained during the impact-echo tests.

Samples		V_p (m/s)	Thickness (m)	
			Impact-echo	GPR
Grey Granite (barrel vaults)	Stone 1	1282.60	0.56	-
	Stone 2	1297.80	0.58	-
	Stone 3	1286.40	0.56	-
Ochre granite (Spandrel walls)	Stone 4	1137.44	0.51	0.45
	Stone 5	1138.46	0.45	0.45
	Stone 6	1133.55	0.45	0.45

3.2 Material characterization

3.2.1 Sonic testing

In order to obtain the mechanical properties of the two masonries identified during the visual inspection (Section 2.2), several indirect sonic tests were carried out in different areas of the bridge (Figure 13). These tests were performed with the same equipment used in the indirect sonic testing carried out on the stone (Section 3.1.3).

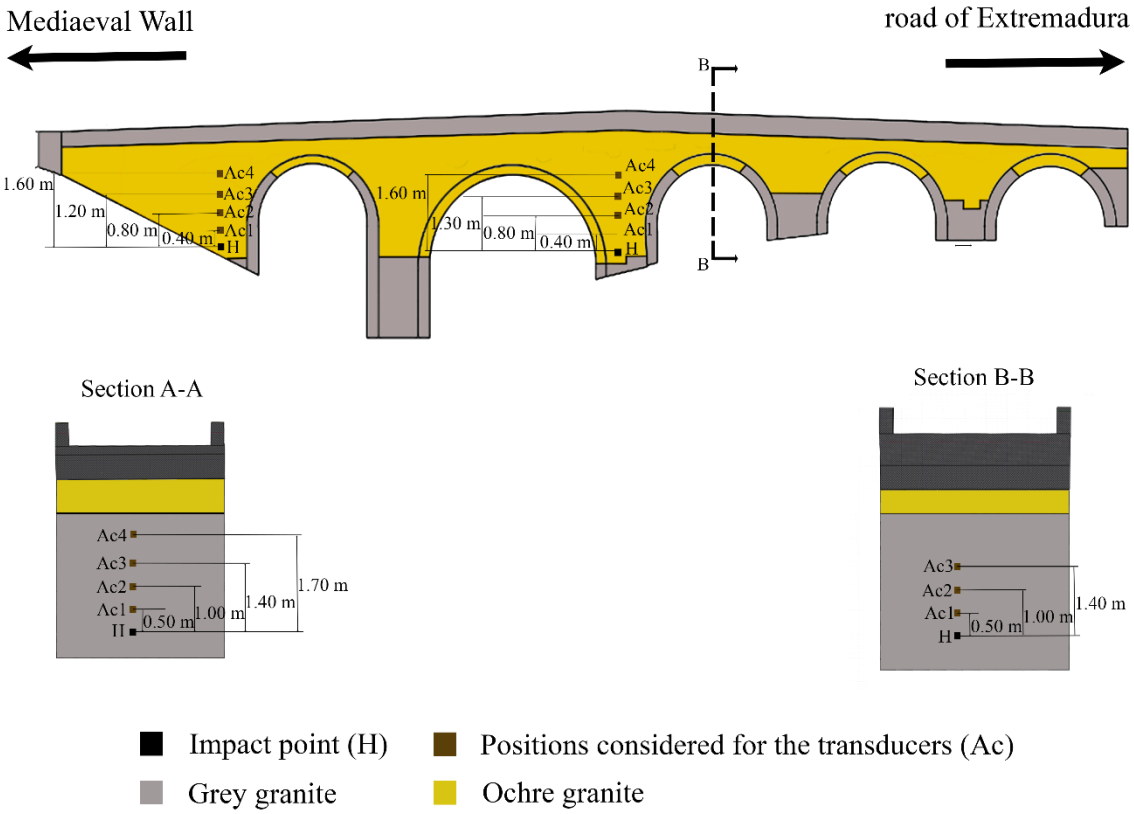

Figure 13: Layout considered for the sonic testing.

On each area evaluated, the material was excited with the instrumental hammer, promoting the generation of compressional or primary waves (V_p) and surface or Rayleigh waves (V_r). The velocity of propagation of these waves was obtained by measuring the time delay between the emission of the signal (impact of the instrumental hammer) and its reception by the transducer. Once the propagation velocity was estimated, it was possible to calculate the mechanical properties of the grey and ochre granite masonries using the following equations (Eq. 2-4) [43]:

$$V_P = \left(\frac{\mathrm{E}\,(1-\nu)}{\rho(1-\nu)(1-2\nu)}\right)^{1/2} \quad (2)$$

$$V_r = \frac{0.87+1.12\nu}{1+\nu}\left(\frac{\mathrm{E}}{2\rho(1+\nu)}\right)^{1/2} \quad (3)$$

$$\frac{V_p}{V_r} = \frac{0.87+1.12\nu}{1+\nu}\left(\frac{(1-2\nu)}{2(1-\nu)}\right)^{1/2} \quad (4)$$

where V_p is the velocity of propagation of the P-waves in m/s; V_r is the velocity of propagation of the R-waves in m/s; E is the Young´s Modulus of the material in GPa; ρ is the density of the material in kg/m3 and; ν is the Poisson´s coefficient of the material.

While the Poisson´s ratio can be directly obtained from the relation between V_p and V_r (Eq. 4), the Young´s Modulus of the masonry requires knowing the density (Eq. 2-3). The density of the grey granite masonry was assumed between 2000 kg/m^3 to 2500 kg/m^3 [19]. Meanwhile, the density of the ochre granite masonry was assumed between 1700 kg/m^3 to 2000 kg/m^3. This assumption was based on the experimental tests carried out by Garcia-Talegon et al. [39] on the ochre granite of Ávila.

Table 4 shows the results of the indirect sonic tests carried out on the masonries. On the one hand, the grey masonry showed average propagation velocities values of 1316.56 m/s and 697.78 m/s for the P and R-waves, respectively, yielding a Young Modulus comprised between 2.90 and 3.60 GPa. On the other hand, lower propagation speeds from the ochre masonry were received (1202.69 m/s for the P-waves and 601.51 m/s for the R-waves) and therefore, a lower Young Modulus, which ranged from 2.05 GPa to 2.41 GPa.

Table 4. Results obtained from the indirect sonic tests.

	Ochre granite		Grey granite	
	P-wave	R-wave	P-wave	R-wave
Average velocity (m/s)	1202.69	601.51	1316.56	697.78
CoV (%)	1.42	1.79	1.48	1.57
Poisson´s coefficient	0.26		0.24	
Density (kg / m3)	1700-2000		2000-2500	
Young´s Modulus (GPa)	2.05-2.41		2.90-3.60	

3.2.2 Multichannel analysis of surface waves

The infill material of a masonry arch bridge can be considered as a soil inserted within the space delimited by the spandrel walls, vaults, and piers. Under this assumption, Geophysics can offer a wide variety of techniques able to characterize soils from a geometrical, physical and mechanical point of view [44]. Within this context, the multichannel analysis of surface waves (MASW) is highlighted. This approach allows obtaining a 2D profile, represented by the plane generated between the geophones, the instrumental hammer and the *z* direction) of the phase velocities and frequencies of the

446 waves generated after the excitation of a soil (dispersion curve) [45]. The fundamental
447 mode of the dispersion curve is extracted and an optimization process, also called
448 inversion analysis, is carried out with the aim of obtaining the shear-wave velocities of
449 the soil (V_s) [46]. Additionally, it is possible to capture the primary-wave velocities (V_p)
450 generated during the excitation of the soil [45]. Thus, the MASW method allow to obtain
451 a 2D plot of the average shear and primary-wave velocities of a soil whit respect to the
452 position of the linear array of geophones and the z axis. Then, both velocities are linked
453 with the Young Modulus and density of the soil as follows (Eq. 5-6):
454

$$\rho = 1.2475 + 0.399\left({}^{V_p}/_{1000}\right) - 0.026\left({}^{V_p}/_{1000}\right)^2 \tag{5}$$

$$E = \rho V_s^2 \frac{3\left(\frac{V_p}{V_s}\right)^2 - 4}{\left(\frac{V_p}{V_s}\right)^2 - 1} \tag{6}$$

455
456 where ρ is the density in kg/m^3; E is the Young´s Modulus in GPa; V_p is the primary-
457 wave velocity of the soil in m/s and; V_s is the shear-wave velocity of the soil in m/s.
458

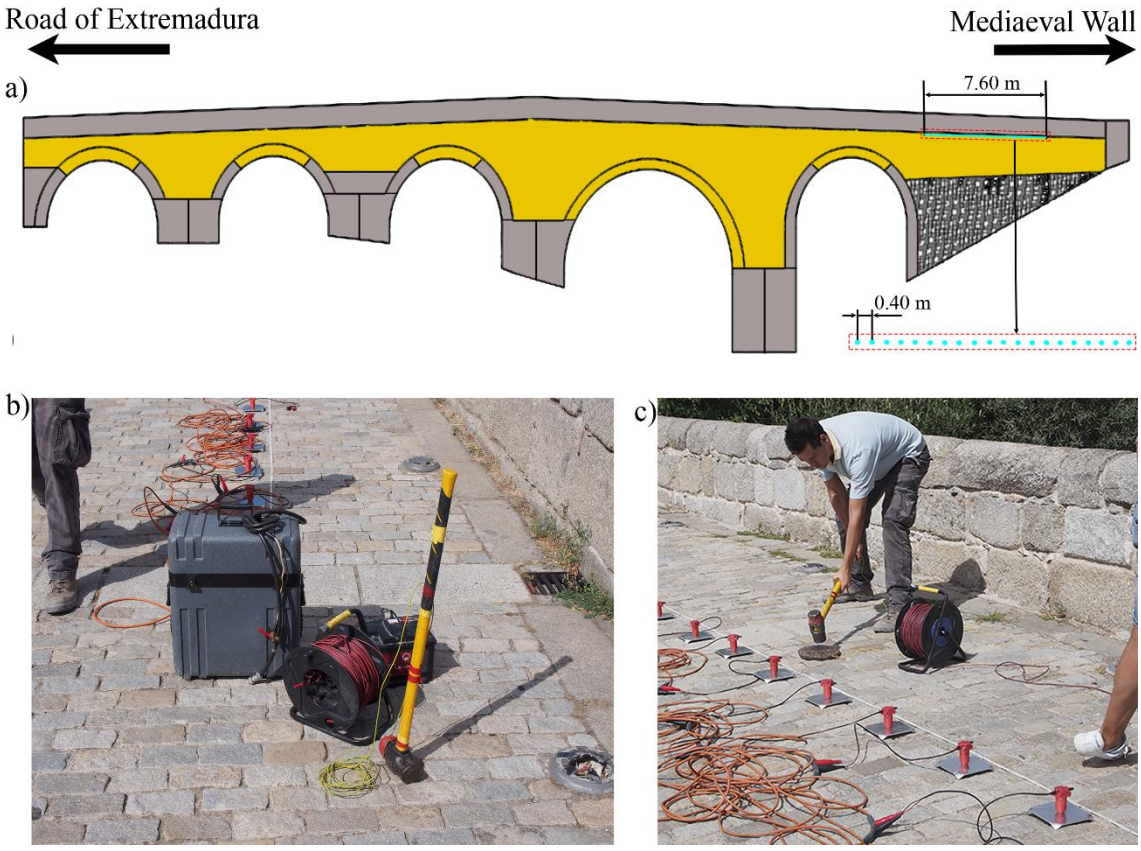

459

460 **Figure 14.** MASW tests: a) setup; b) detail of the used equipment and; c) instant of when the infill is
461 excited. In blue the array of geophones used during this test.

Taking into account all the above mentioned, a MASW test was carried out on the east part of the bridge (Medieval Wall) (Figure 14a). The excitation of the soil was carried out using a 20.00 kg tenderizer connected to a data acquisition unit (Figure 14b) (Figure 14c). The excitation was captured by a linear array of 20 geophones equally spaced (0.40 between each one of them in a total length of 7.60 m) (Figure 14a) and connected to the data acquisition unit.

Table 5 shows the results obtained from the MASW test. From the Vs values it was possible to obtain a first estimation of the bridge infill layers (Figure 15)(Table 5): i) one layer, with a depth of approximately 1.76 m, made up by a compacted material with an average Young´s Modulus of 0.43 GPa and; ii) a second infill layer with an average Young´s Modulus of 1.03 GPa, ranging from the final of the first infill layer until the foundation of the bridge. These values seem to be consistent with both those obtained by the archaeological samples (Section 2.2) as well as with the values found in the existing literature [8, 47, 48].

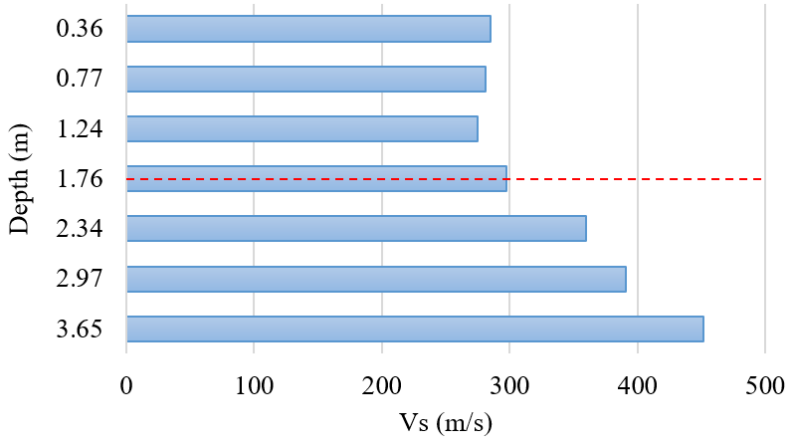

Figure 15. Graphical representation of the relation between the depth and the V_s speeds. The red line represents the interface between the different bridge´s infill layers.

Table 5. Values obtained for the two infill layers identified on the bridge. UB denotes the upper bound value and LB the lower bound value.

	First layer		Second layer	
	UB	LB	UB	LB
V_p (m/s)	1451.4	1427.3	1705.2	1606.7
V_s (m/s)	316.1	294.7	515.0	419.6
E (GPa)	0.52	0.45	0.84	1.28
ρ (kg/m3)	1771	1764	1852	1821

3.3 Dynamic identification

With the aim of identifying the dynamic properties of the bridge (natural frequencies and modal displacements), an ambient vibration test (AVT) was also performed in the last stage of the in-situ non-destructive survey. To achieve reliable results, several numerical simulations, adopting different boundary conditions, were previously performed. In this

way, it was possible to arrange the most proper configuration for the AVT test as well as the identification of the most appropriate areas to place the accelerometers (Figure 16). To extract the dynamic properties of the bridge, the Enhanced Frequency Domain Decomposition algorithm (EFDD), based on the power spectral density, was applied [49]. Consequently, a total of seven mode shapes were successfully identified together with its corresponding frequencies, ranging between 10.29 Hz to 31.90 Hz [8] (Table 6).

For this case study, it is worth mentioning the high frequencies obtained in comparison with similar tests carried out in other masonry bridges (Table 6). These values are suggestive of a structure with a high stiffness/mass ratio which can be explained by the presence of a reinforced concrete slab on the deck, a high-quality infill and the use of a light-weight masonry (ochre granite).

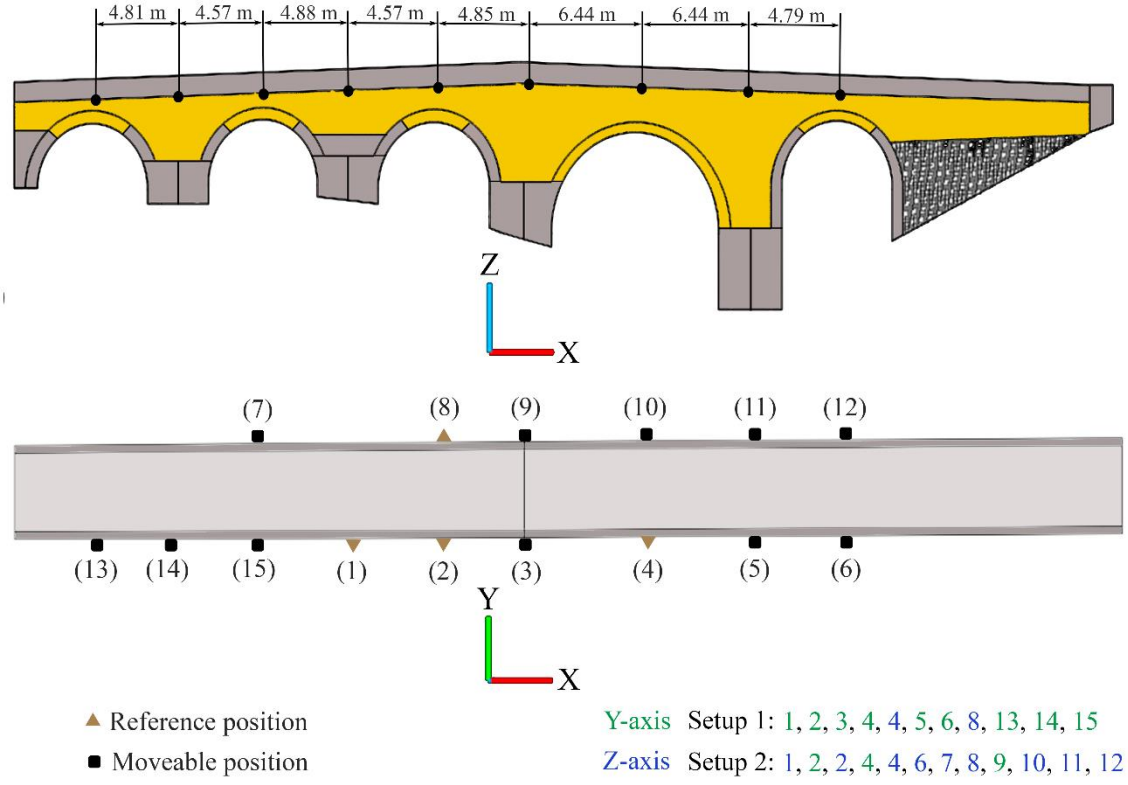

Figure 16. Schematic representation of the setups carried out during the AVT test.

Table 6: Natural frequencies and mode shapes obtained from the AVT tests

Mode	Natural frequency (Hz)	Description of the modal shape
1	10.30	Translational mode in the *x* axis
2	14.57	Torsional model in the *x* axis
3	21.09	Translational mode in the *z* axis
4	24.13	Torsional model in the *y* axis
5	26.31	Torsional and translational mode in the *x* and *z* axis respectively

6	29.45	Torsional model in the *x* axis
7	31.90	Torsional modle in the *y* and *x* axis

506

507 It is worth mentioning that the accelerometers used to capture the dynamic response of
508 the bridge were placed mainly in the z and the y direction in order to capture the weak
509 direction (out-of-plane) as well as the vertical response of the structure. This type of setup
510 is similar to those adopted in other experimental campaigns [8, 16].
511

512 # 4 Numerical model

513 ## 4.1 Point cloud registration

514 Previous to the generation of the geometrical CAD model, the registration strategy
515 defined by Bautista-De Castro et al. [12] was applied. This approach allows registering
516 the longitudinal axis of the bridge´s point cloud with the *x*-axis of the global coordinate
517 system, and thus the correct integration of the different data captured (e.g., AVT). To this
518 end, the following steps were carried out (Figure 17): i) extraction of the covariance
519 matrix (Eq. 7-8); ii) Eigenvalue analysis of the covariance matrix (Eq. 9); iii) evaluation
520 of the angle between the Eigenvector associated with the maximum Eigenvalue and the
521 *x*-axis of the global coordinate system and; iv) a *z* rotation of the global point cloud.
522

$$C = \frac{\sum_{p_i \in P} w_i (p_i - \bar{p})^T (p_i - \bar{p})}{\sum_{i=1}^{n} w_i} \tag{7}$$

$$\bar{p} = \sum_{i=1}^{n} p_i / n \tag{8}$$

$$V^{-1} C V = D \tag{9}$$

523
524 where C is the covariance matrix of the point cloud P; w_i is the weight associated to each
525 point p_i; $\bar{p}$ represents the mean of the points; V is an orthogonal matrix that contains the
526 corresponding eigenvectors and; D is the diagonal matrix containing the eigenvalues. For
527 the present case study, the same unit weight was assumed for each point.
528

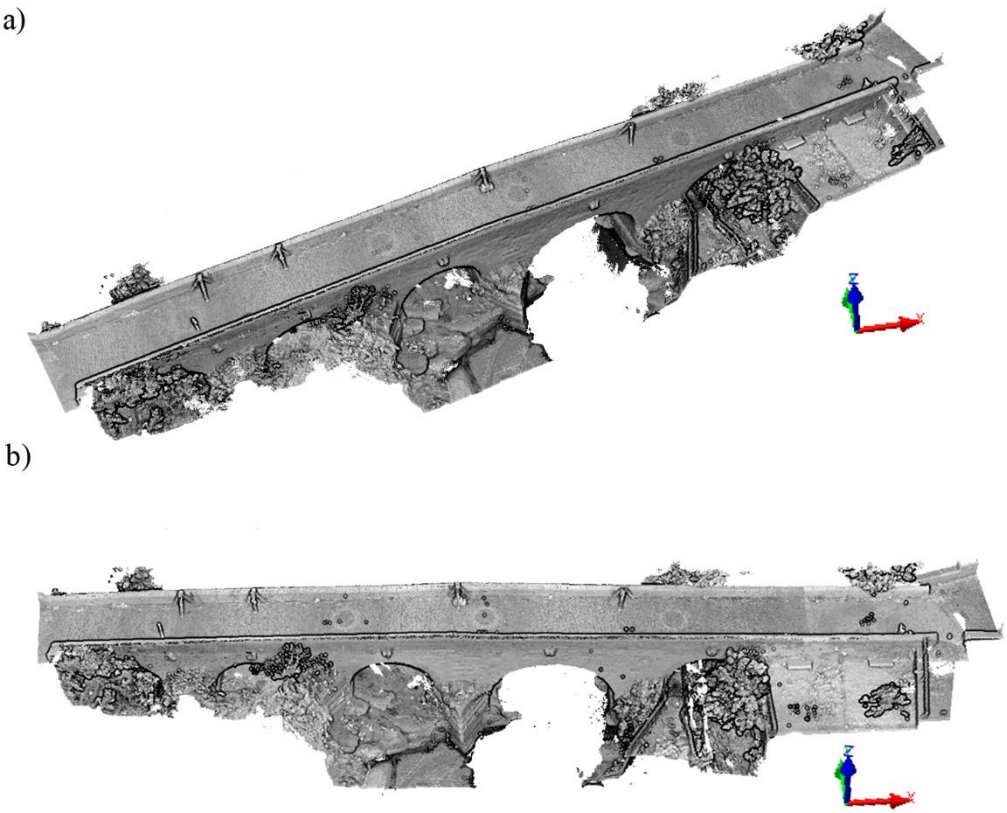

Figure 17. Point cloud of the bridge: a) before registration and; b) after registration. The longitudinal axis of the bridge after the registration corresponds with the *x*-axis of the global coordinate system.

4.2 Creation of the as-built CAD model

According to Sánchez-Aparicio et al. [25], the creation of a suitable CAD model for numerical analysis purposes can be carried out by means of the following strategies: i) extraction of orthogonal views and sections over several directions of the point cloud or mesh or; ii) by means of advanced surface representation methods such as the non-uniform b-splines, allowing the representation of complex surfaces. Taking into consideration the out-of-plane deformations observed during the visual inspection (Section 2.3), the second approach was deemed as the most adequate, being carried out through the following workflow (Figure 18): i) 3D Delaunay triangulation; ii) extraction of sections, spaced 1.00 m, along the *x*-axis; iii) vectorization of each section by means of b-splines curves and; iv) creation of a solid geometrical model based on Loft surfaces, considering the b-splines as its directrix curves [50].

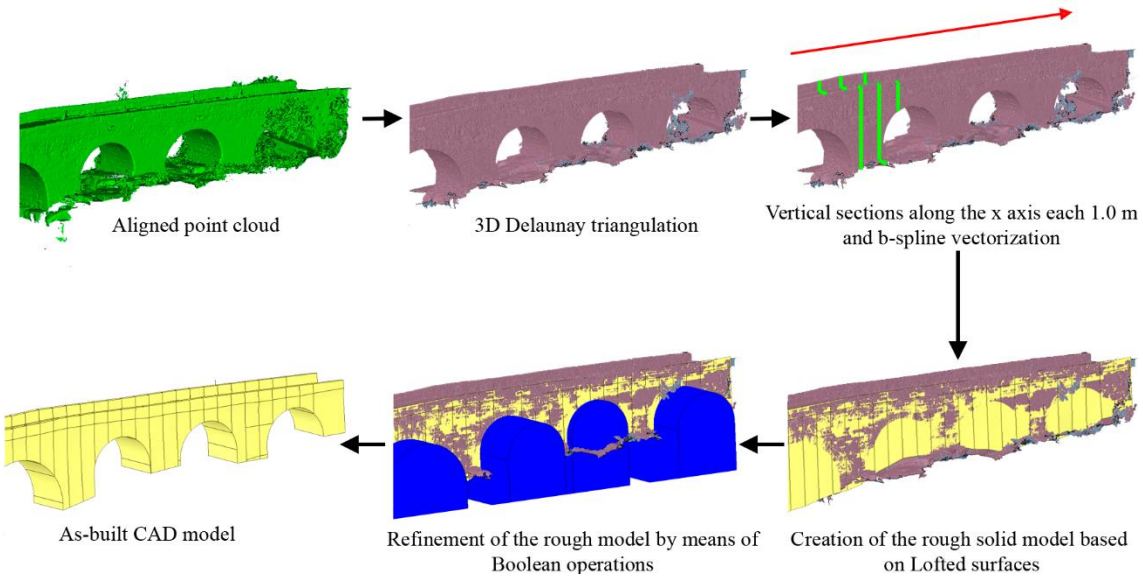

Figure 18. Proposed workflow for the generation of the as-built CAD model.

As a result, it was possible to construct a rough solid model of the bridge envelope on which the out-of-plane deformations observed on the spandrel walls were accurately captured. To refine this model, including the barrel vaults and other bridge elements such as the infill layers, several Boolean operations were posteriorly carried out [50], intersecting parametric shapes (e.g., cylinders for the barrel vaults and planes for the definition of the boundaries and materials) with the envelope obtained in the previous stage (Figure 18). It is worth mentioning that the interface between infills was modeled based on the data provided by the GPR and the MASW tests. Meanwhile, the thickness of the spandrel walls was modeled assuming a fixed average value, estimated in 0.46 m, obtained from the vertical GPR profiles as well as the impact-echo tests (Table 3).
The reverse engineering procedure previously defined allowed obtaining a highly detailed solid CAD model. However, and considering the focus of the present study, the creation of an accurate numerical model of the bridge, the cutwaters were omitted at this stage and later integrated during the generation of the finite element mesh.

4.3 Finite element mesh

Departing from the geometrical model previously created, a finite element mesh was generated using the FEM software TNO Diana® [51] (Figure 19). This mesh was composed by 86,418 solid elements and 166,292 degrees of freedom, including two elements along the thickness of the spandrel walls and barrel vaults in order to correctly capture stress gradients in subsequent non-linear structural analysis. It is worth mentioning that the cutwaters were defined through extrusions, considering a geometry with an equivalent stiffness (Figure 19). The concrete slab, as well as the granite cobblestone, were included into the model by means of extrusion of the bridge´s deck. These extrusions were made without any connection with the spandrel walls as it was observed during the visual inspection.
Concerning the boundary conditions, they were applied in agreement with the surrounding medium of the bridge: pinned supports at the base, abutments, and the spandrel wall covered by the soil added in 1995 (Figure 4) (Figure 5).

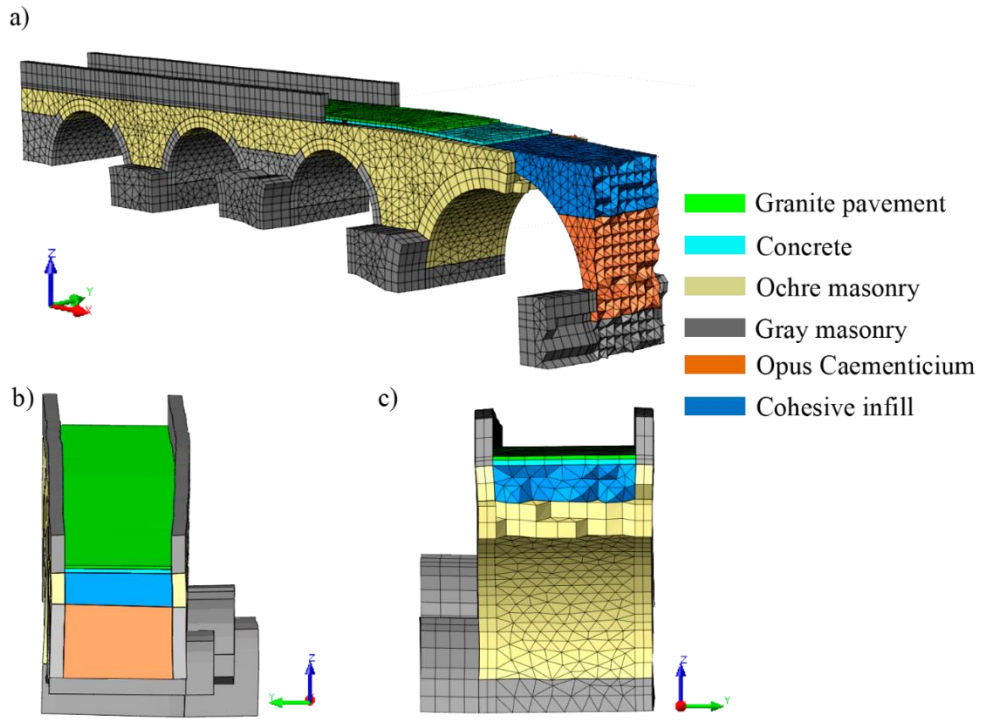

Figure 19. Finite element mesh: a) general view; b) and c) details of the mesh on which is possible to observe the real captured geometry of the spandrel walls.

As for the material properties of the masonry and infill, they were defined according to the values obtained during the experimental campaign (Table 7) (Table 8). Meanwhile, the materials of the bridge´s deck were defined according to the data provided by the last restoration project (Table 9): a granite cobblestone pavement joined with a cement mortar upon a concrete slab. On the one hand, the homogenized Young´s Modulus of the granite cobblestone was set according to the equations defined by the Eurocode 6 [52] and the experimental data obtained by Garcia-Talegón et al. [53]. On the other hand, the mechanical and physical properties of the concrete slab were defined according to the Eurocode 2 [54], considering a characteristic compressive strength of 16 N/mm^2 (C 16/20). It is worth mentioning that the steel bars detected by means of the horizontal radargrams were not included in the numerical simulation since they not have a structural function.

Table 7. Mechanical properties of the masonries.

Material	Variable	Upper bound	Average value	Lower bound
Grey granite masonry	Young Modulus (GPa)	3.60	3.25	2.90
	Poisson ratio (-)	-	0.24	-
	Density (kg/m3)	2500	2250	2000
Ochre granite masonry	Young Modulus (GPa)	2.41	2.23	2.05
	Poisson ratio (-)	-	0.26	-

	Density (kg/m3)	2000	1850	1700

596

597 **Table 8.** Mechanical properties of the infill material layers.

Layer	Variable	Upper bound	Average value	Lower bound
1 (cohesive material)	Young Modulus (GPa)	0.52	0.48	0.45
	Poisson ratio (-)	-	0.20	-
	Density (kg/m3)	1771	1768	1764
2 (opus caementicium)	Young Modulus (GPa)	1.28	1.03	0.84
	Poisson ratio (-)	-	0.05	-
	Density (kg/m3)	1852	1837	1821

598

599 **Table 9.** Mechanical properties of the materials of the bridge´s deck.

Material	Variable	Upper bound	Average value	Lower bound
Concrete slab	Young Modulus (GPa)	-	25.70	-
	Poisson ratio (-)	-	0.20	-
	Density (kg/m3)	-	2400	-
Granite cobblestone	Young Modulus (GPa)	-	16.78	-
	Poisson ratio (-)	-	0.20	-
	Density (kg/m3)	-	2318	-

600

601 # 5 Evaluation of the discrepancies between the numerical model and the
602 # experimental modal data

603 One of the factors explaining the widespread employment of the FEM method in the
604 analysis of masonry structures is the possibility of simulating complex scenarios such as
605 earthquakes or settlements. However, the quality of the output results obtained from these
606 simulations is strongly influenced by the uncertainties associated with the mechanical
607 properties of the materials, the correct definition of the boundary conditions of the
608 structure and the geometrical simplifications incurred when developing the numerical
609 model. Therefore, these aspects demand the use of suitable strategies able to validate these
610 numerical simulations .
611 Taking all of this into account, a preliminary numerical simulation (eigen-value analysis)
612 was carried out with the average values of the different materials present on the structure
613 (Table 7) (Table 8) (Table 9). In order to evaluate the accuracy of the numerical
614 simulation, it was considered as quality indicators the error between frequencies and the
615 modal assurance criterion (MAC) [55] (Table 10).
616

617 **Table 10**. Results obtained from the initial numerical simulation.

Mode	Experimental frequency	Numerical frequency	MAC
1	10.30	9.62	0.97
2	14.57	14.39	0.85

3	21.09	20.00	0.97
4	24.13	-	-
5	26.31	24.39	0.94
6	29.45	28.34	0.83
7	31.90	29.95	0.55

The results obtained from this initial numerical simulation showed a more flexible structure in comparison with the real one (with an average error in frequencies of 5.03%), suggesting the need of performing a calibration or model updating procedure to improve the discrepancies (Table 10). As for the MAC values, it was possible to observe a fairly good match at the exception of the 7th mode.

Thereby, manual calibration of the numerical model was carried out by modifying the Young´s Modulus of the infill layers and masonries within the allowable range of values determined by the upper and lower bounds received from the experimental campaign (Table 7) (Table 8). Moreover, to mimic the real response of the structure with greater fidelity, it was considered a possible interaction effect between the east part of the bridge and the infill soil added in 1996. For this particular case, it was defined a range of admissible stiffness comprised between $1x10^7$ N/m^3 and $1x10^9$ N/m^3 according to Bautista-De Castro et al. [12]. As a result, it was possible to obtain a numerical simulation whose dynamic response closely matched the dynamic response captured by the AVT tests (Table 11) (Table 12) (Figure 20). Thus, the updated numerical model showed an average error in frequencies of 2.22 % and an average modal assurance criterion of 0.91 (Table 12).

It is worth mentioning the asymmetric dynamic response of the bridge in the Mode I and II. This phenomenon can be attributed to the structural disposition of the bridge on which the major barrel vault, which has 1.5 more thickness and 3 times more length in terms of spam (Table 1), is not centered with respect to the structure (Figure 4).

Table 11. Updated values obtained after the manual calibration. UB and LB denotes the upper and lower bounds respectively.

	Variable	UB	LB	Update value
Grey granite masonry	Young Modulus (GPa)	3.60	2.90	3.60
Ochre granite masonry	Young Modulus (GPa)	2.41	2.05	2.41
Cohesive infill	Young Modulus (GPa)	0.52	0.45	0.50
Opus Caementicium	Young Modulus (GPa)	1.28	0.84	1.28
Interaction soil-bridge	Tangential stiffness in the longitudinal direction (N/m3)	$1x10^9$	$1x10^7$	$1x10^9$
	Tangential stiffness in the transversal direction (N/m3)	$1x10^9$	$1x10^7$	$1x10^9$

643

644 **Table 12.** Results obtained from the updated numerical model.

Mode	Experimental frequency	Numerical frequency	MAC
1	10.30	10.02	0.98
2	14.57	14.95	0.87
3	21.09	20.76	0.96
4	24.13	-	-
5	26.31	25.11	0.95
6	29.45	29.81	0.86
7	31.90	32.11	0.86

645

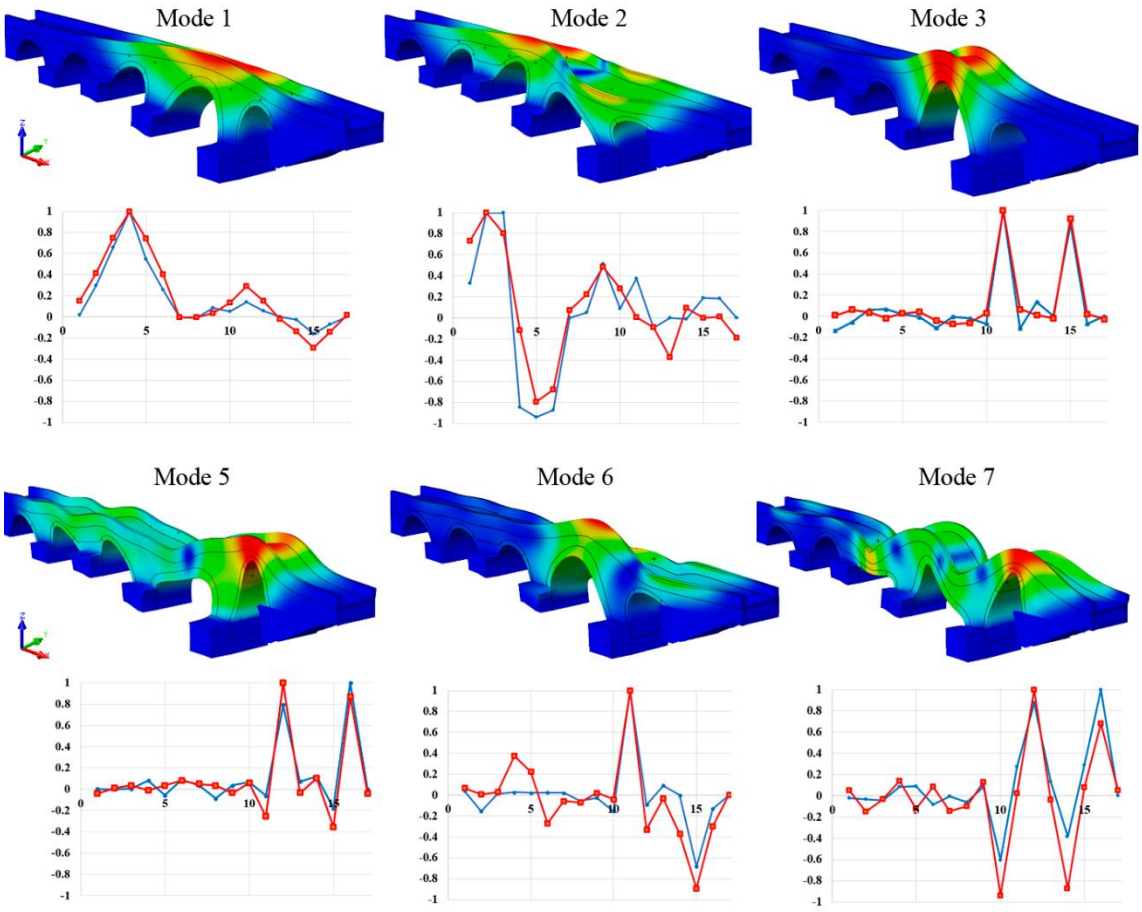

646

647 **Figure 20.** Results obtained after the manual calibration carried out. The red lines in the graphs represents
648 the numerical normalized modal displacements. Meanwhile the blue lines represent the experimental
649 normalized modal displacements.

650 The good quality of masonry as well as the well-shaped ashlars found in the spandrel
651 walls, cutwaters and vaults are consistent with the values obtained during the sonic tests
652 and the calibration of the numerical model (Figure 4b) (Figure 4c) (Table 12). As
653 expected, the calibration procedure pointed out a non-negligible interaction effect
654 between the soil added in 1995 and the east part of the bridge (Figure 1b) (Table 12).
655 Finally, regarding the infill layers, it was possible to corroborate again the presence of a
656 high-quality infill material in the most part of the structure, which lays in the Roman

origin of the bridge, and which is also consistent with the data provided by the archaeological samples taken during 1995.

6 Structural assessment

6.1 Modeling assumptions

In the developed computational model, the non-linear behavior of the masonries (grey and ochre granite) was modeled by adopting the total strain rotating crack model (TSRCM), implemented in the Finite Element software TNO Diana [51]. A post-peak exponential softening for tensile behavior and a parabolic hardening followed by a post-peak parabolic and exponential softening for compression were respectively adopted. To estimate the inelastic parameters describing the masonry nonlinear behavior, the following criteria was considered for both types of masonries: i) the compressive strength value was considered as 1000 times the corresponding Young's Modulus, as proposed by Tomazevic et al. [56]; ii) for the fracture energy in compression it was adopted a ductility index of 1.60 mm [57]; iii) the tensile strength was taken equal to 5.00% of the compressive strength and; iv) the fracture energy in the tensile regime was assumed as 0.05 N/mm.

The infill layers were modeled obeying to a Mohr-Coulomb failure criterion. For the infill added during the Mediaeval period, it was considered the values proposed by Conde et al., i.e., a friction angle of 30º together with a cohesion of 20 kPa. On the other hand, the *Opus Caementecium* was modeled according to the values proposed by Frunzio et al. [47], i.e., a friction angle of 32º and a cohesion value of 500 kPa.

For the concrete slab added during the last restoration project (see Section 2.1) it was considered a compressive strength of 16.00 N/mm^2 and a tensile strength of 1.90 N/mm^2 according to the Eurocode 2 [58]. Due to the complexity of the model, and the almost null contribution to the overall structural response of the bridge, the granite cobblestone was not explicitly modeled. However, in an attempt to still partially consider it, the mass of this element was added as an external load over the concrete slab. This load had a value of 2.30 kN/m^2.

To obtain the solution of the non-linear problem, the regular (full) Newton-Raphson method was used. Complementary to this, the line-search technique and the arc-length method in a spherical path. It is worth mentioning that th. As for the convergence criterion, an energy norm was adopted with a threshold value of 0.001.

6.2 Safety analysis against vertical loading

To evaluate the mechanical performance of the bridge, both a non-linear analysis under its self-weight and under an increasing gravitational loading were performed. Both aspects will allow evaluating the current safety condition of the structure against vertical loads. It is noted that the bridge is currently closed to the traffic and in an area with a low seismic hazard. Thus, no analysis under live loads or seismic loading were taken into account within the framework of the present study. During this numerical simulation, the control node used to track the response of the structure was placed at the mid-line and mid-span of the barrel vault with the higher rise to span ratio (vault number 4).

Two different models were used in the numerical simulation procedure, which are categorized as follows: a) Model I: for the analysis of the bridge behavior under its self-weight and; b) Model II: for the evaluation of the performance of the structure under vertical loads.

Thus, concerning the structural behavior of the bridge against its self-weight (Model I), it was observed that the minimum principal (compressive) stresses appeared on an area close to pier number 4, at the springings of the major barrel vault (Figure 21). The maximum value was around 0.68 MPa, which is pretty far away, 19.00%, of the maximum compressive capacity estimated for the grey granite masonry (around 3.60 MPa). As expected, at this load status the bridge is fundamentally under compression everywhere. Areas with tensile stresses are rather localized, particularly at the upper part of spandrel walls as well as at the mid-span of all barrel vaults. The maximum value for these stresses was approximately 0.10 MPa.

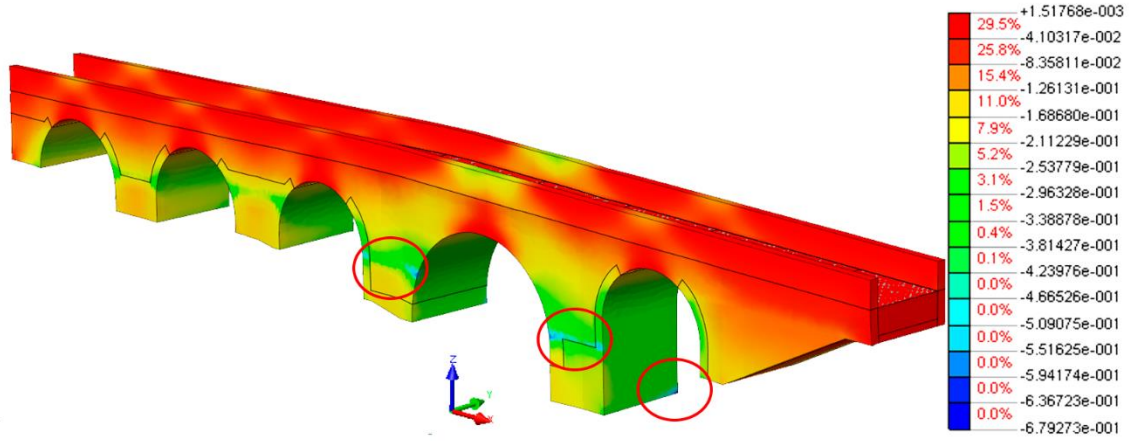

Figure 21: Contour plot of minimum principal stresses obtained for the Model I (MPa).

For the case of the Model II, the gravity load was monotonically increased until causing the collapse of the bridge. As a result, the bridge was able to withstand up to seven times its own weight (Figure 22**¡Error! No se encuentra el origen de la referencia.**). This safety factor seems to be related with the high-quality of the different constructive elements (masonry and infill), the weather-tightening concrete placed on the deck (Table 11) and the dimensions of the structure (Table 1). The failure mechanism of the structure appears on the area placed between the barrel vaults 3-4-5. In this zone it is observed a bending failure of the spandrel wall between the vaults 3-4 and 4-5 as a consequence of an excessive lateral pressure due to the failure of the infill. It is possible to observe a failure of the vault 4 and a partial failure of the vault 3 due to the excessive lateral pressure produced as a consequence of the infill failure (Figure 23a). Regarding the compression status it is possible to observe some crushing problems in the lower part of the pier that stand the barrel vault 4 and 5 as well as the lower part of the barrel vault 3 (Figure 23b). According with this analysis (despite the intrinsic uncertainties associated with the accurate determination of the inelastic parameter values), the bridge mechanical performance under vertical loads is fairly satisfactory. The results obtained, in absence of specific numerical analysis, suggest that the bridge could stand traffic.

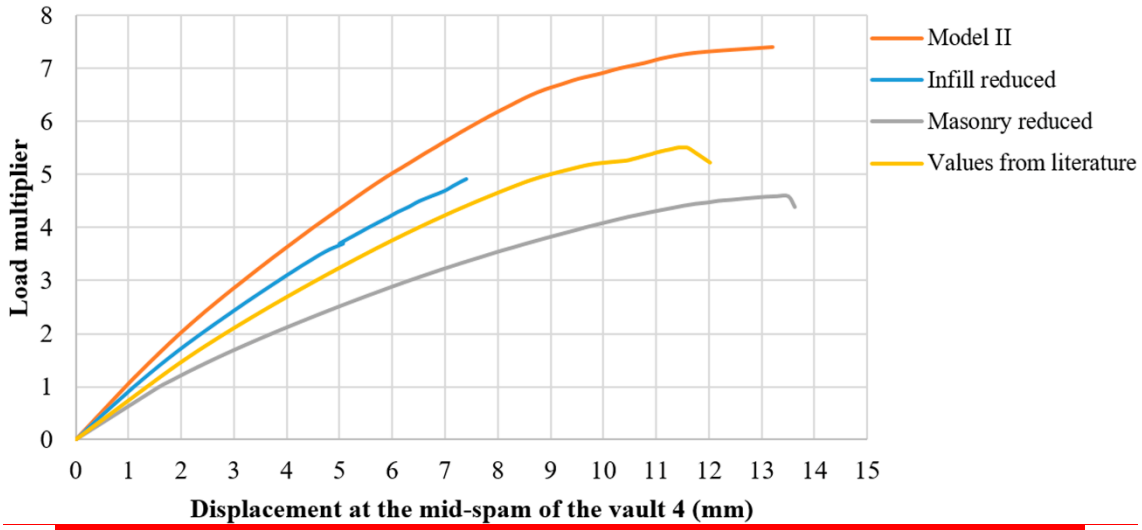

Figure 22: Load-displacement curves obtained. In orange the response of the bridge in its current configuration. In blue the response of the bridge in case of considering the mechanical properties provided by the literature. In green and in grey the response of the structure in case of reducing by half the masonry and infill properties respectively.

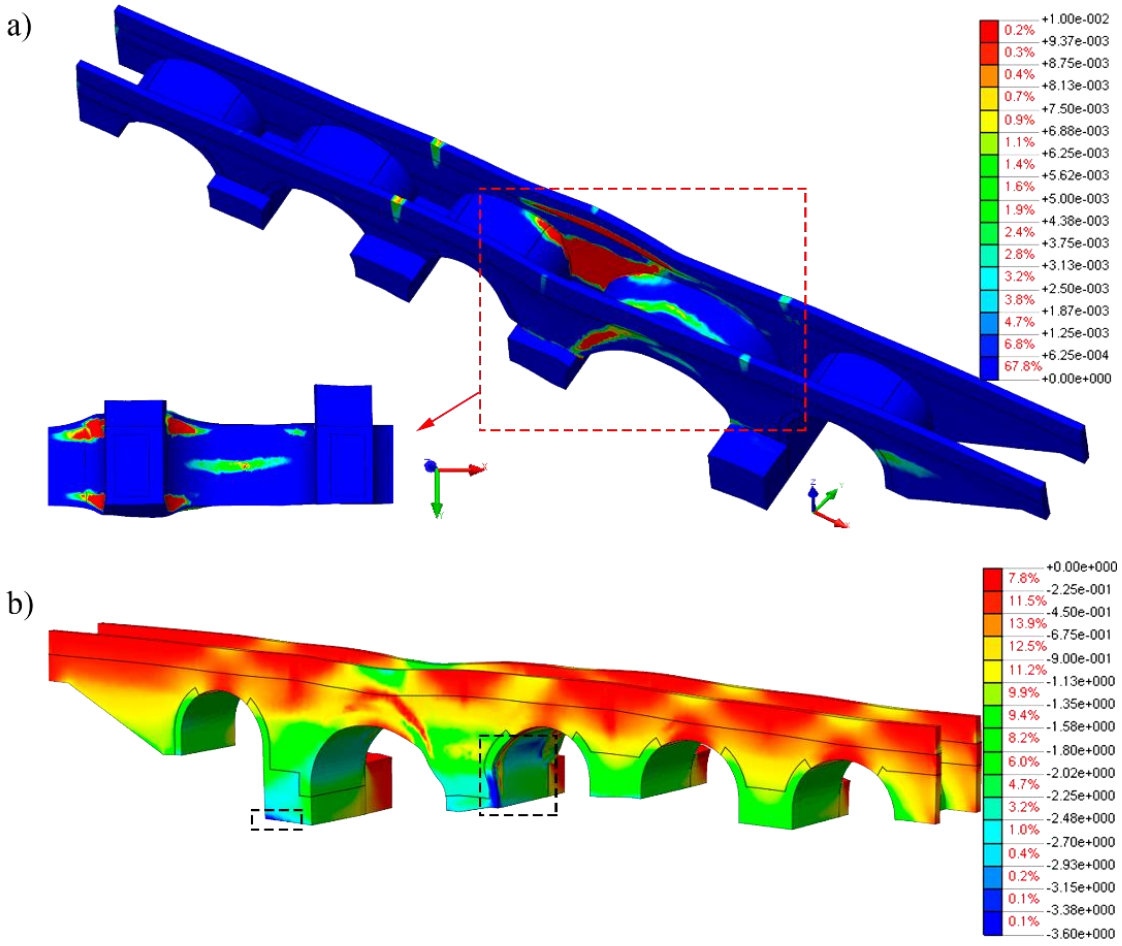

Figure 23: Deformed shape at faliure due to the incremented gravitational loading: a) contour plot of màximum principal strains (indicator of cracking) and; b) contour plot of minimum principal stresses.

Taking into consideration the focus of the present work: the propose of a multidisciplinary approach able to characterize masonry bridges at geometrical, material and structural level, a comparative study was carried out. This study has the aim of confronting the

results obtained by the proposed methodology with those obtained in case of considering the values provided by the literature. In this case it was considered the values provided by the Italian code NTC08 [59]. This code provides ranges of material properties for different masonry typologies. Both masonries were encapsulated within the class ashlar stone masonry, assuming a Young Modulus of 2.4 GPa for the ochre masonry and 3.2 GPa for the grey masonry. For the infill it was considered the average values proposed by Conde et al. [8] and Frunzio et al. [47] for the cohesive infill and the *Opus Caementicium* respectively. Since these values comes from the literature a structural knowledge level of LC1 has been assumed, with a consequent confidence factor equal to 1.35 [59].

In case of considering the values provided by the literature the safety factor of the bridge against vertical loads decreases from 7.3 to 5.5 (25% less). It is worth mentioning that the failure mechanism shows some discrepancies. In case of considering the values provided by the literature the damages within the tensile regimen appears concentrated in the vault 4 (instead of the vault 3 and 4) (Figure 24a). Regarding the compression regime, it was possible to observe a similarity between both models (Figure 24b).

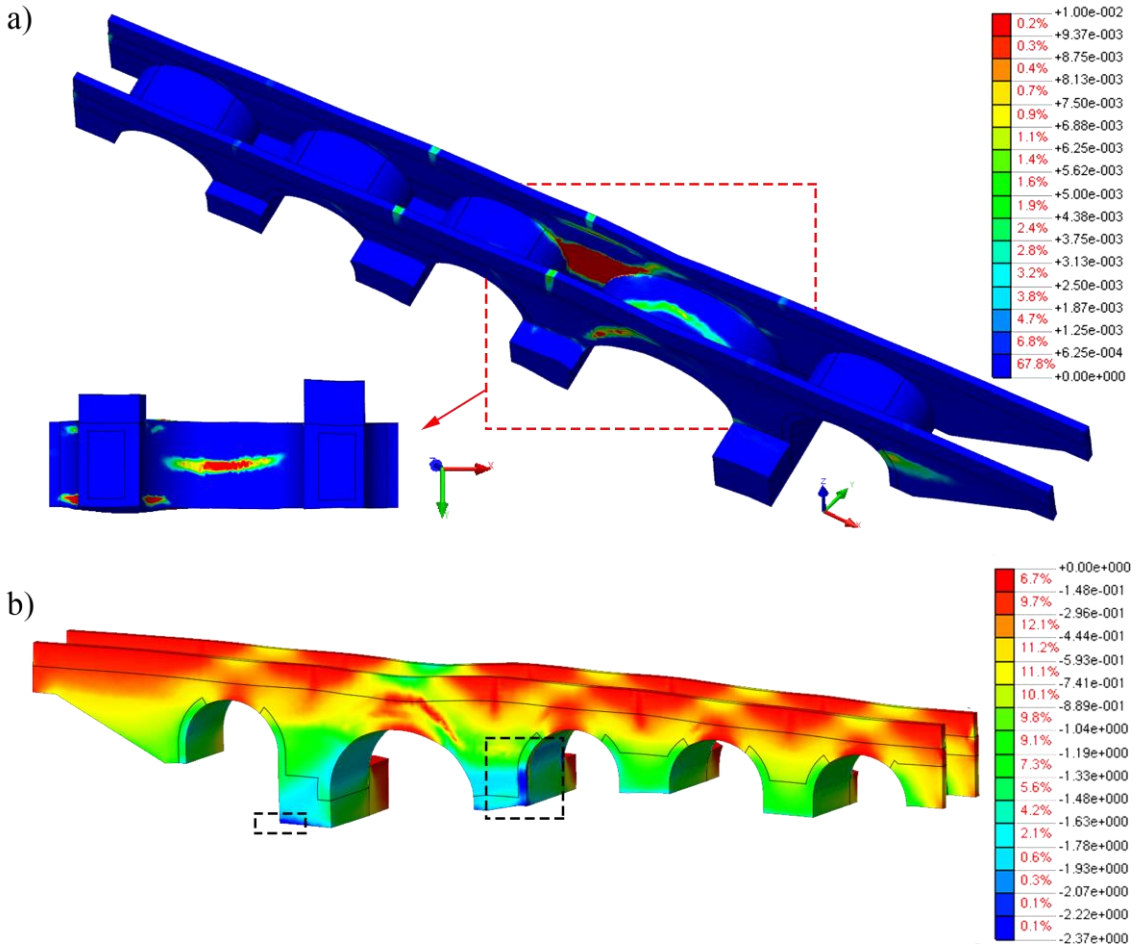

Figure 24: Results from the numerical model made up by the values provided by the literature: a) contour plot of maximum principal strains (indicator of cracking) and; b) contour plot of minimum principal stresses.

Additionally, several numerical simulations were carried out with the aim of evaluating the influence of the main structural components, namely masonry and infill, in the global

response of the structure. To this end, the mechanical properties of each component were reduced by half (Figure 22). According with this results, it is possible to observe that both properties have a similar impact in the final safety factor, reducing one of them by a half decrease the safety factor of the bridge in about 34%. In spite of this similarity in terms of safety factor, it was possible to observe that a reduction of the masonry properties promotes a more ductile response due to the presence of crushing areas (Figure 22).

6.3 Evaluation of the structural response in case of continuing the material looses

One of the main advantages that can offered an accurate numerical simulation, made up by an extensive experimental campaign, is the possibility of simulating the response of the structure against different hazards such as earthquakes, material losses or pier scours. Under this basis, the structure used to validate the proposed multidisciplinary approach was simulated against its more probable hazard: the material loses. To this end, the resistance section of the spandrel walls and vaults were reduced in a 25 and 50 percent (Table 13).

Table 13: Thicknesses of the spandrell walls and barel vaults considered.

Element	Original (m)	Reduction of 25%	Reduction of 50%
Vault 1 (West)	0.55	0.41	0.28
Vault 2	0.54	0.41	0.27
Vault 3	0.53	0.40	0.27
Vault 4	0.85	0.64	0.43
Vault 5 (East)	0.55	0.41	0.28
Spandrel wall	0.45	0.34	0.23

As it was expected if the resistance section is reduced, the bearing capacity of the bridge is lower. On the one hand, if the section is reduced by a 25% the safety factor of the bridge decreases a 13% (from 7.2 to 6.3). On the other hand, if the section is reduced by a 50% the safety factor decreases a 30% (from 7.2 to 5.2) (Figure 25). According with this, in a medium-large term the bridge is safe against material losses, mainly due to the high quality of its materials.

Regarding the collapse mechanism, it was possible to observe some discrepancies with respect to the initial one (Model II). The collapse of the structure in cases of reducing the section by a 25% is mainly focused on the spandrel wall between the barrel vault 3 and 4. However it was possible to observe some cracking on the barrel vault 5 (Figure 26a). On the other hand, the collapse of the structure in case of considering a material loos of 50% is mainly in the tensile regime, collapsing the spandrel wall placed between the barrel vault 3 and 4. Also it was possible to observe a separation of the keystone of the main barrel vault (Figure 26b). With respect to the compressive stresses, the crushing areas were reduced to a small part of the pier.

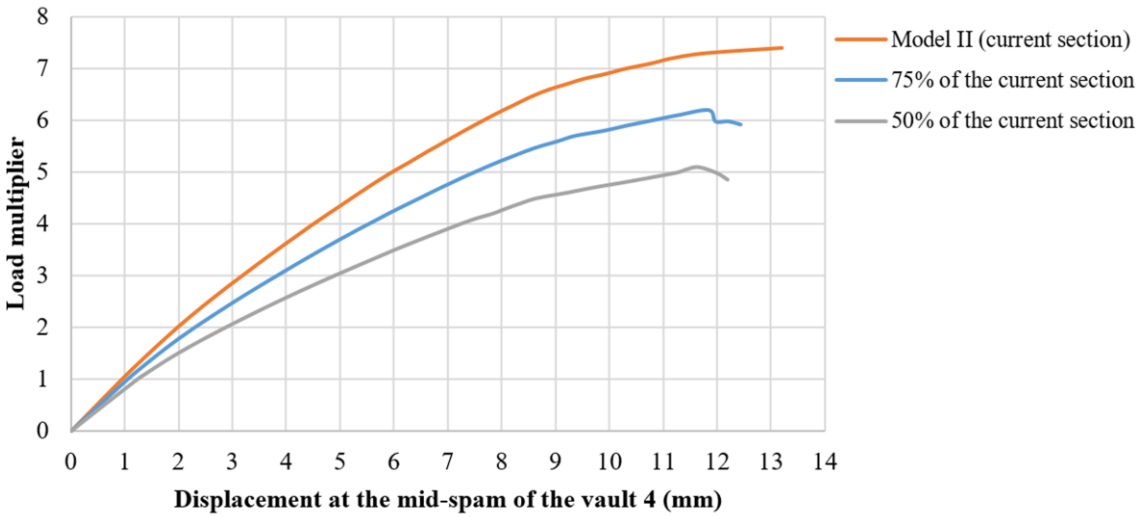

806

807 **Figure 25:** Load displacement curves obtained during the numerical simulations.

808

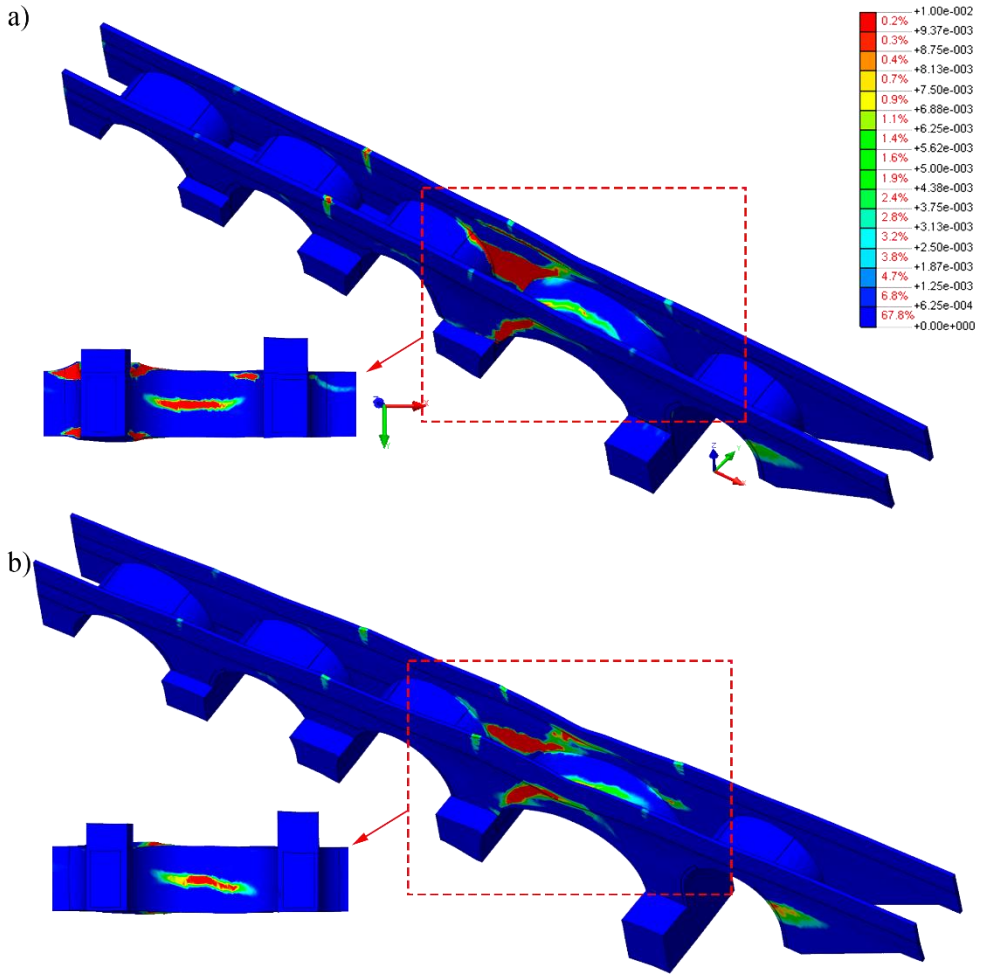

809

810 **Figure 26:** Results of the section reduction: a) 75% of the original one and; b) 50% of the original one.

811 7 Conclusions

812 In this work a fully non-destructive multidisciplinary approach applied to the structural
813 diagnosis of masonry arch bridges is proposed. This methodology allows a

814 characterization of masonry bridges at different levels: i) geometrical level; ii) material
815 level and; iii) structural level.
816 From the geometrical point of view, the method uses several well-known approaches such
817 as the terrestrial laser scanner and the ground penetrating radar. These approaches are
818 complemented by several surface waves technologies such as the impact-echo method
819 and the multichannel analysis of surface waves. The former allows to evaluate the
820 thickness of the different construction elements (e.g. spandrel walls or vaults).
821 Meanwhile, the latter allows to characterize the inner disposition of the bridge´s infill,
822 even in situations on which the ground penetrating radar cannot penetrate. Then, all this
823 data is combined in an as-built CAD model created by means of the last advances in
824 reverse engineering, i.e. extrusions, boolean operations and Loft surfaces. The
825 combination of these methods allow to generate models able to reproduce complex
826 deformations presented in historical constructions.
827 At the material level, the proposed methodology introduces two surface-waves
828 methodologies. On the one hand, it is proposed the sonic testing for the characterization
829 of the elastic properties of the masonry. On the other hand, it is used the multichannel
830 analysis of surface waves for the characterization of the Young Modulus and the density
831 of the infill. This method, based on a linear array of geophones, allow to create 2D profile,
832 made up by shear-velocities, of the bridge´s infill. Both methodologies enable the material
833 characterization of the bridge without needing the use of invasive techniques.
834 Finally, the ambient vibration testing was also adopted as a non-destructive technique
835 able to characterize the global response of masonry arch bridges. Then, this technique is
836 used to detect potential mismatches between the real structure behavior and the simulated
837 one.
838 The combination of all the methodologies previously shown allow to generate accurate
839 advanced numerical simulations of masonry arch bridges. In order to evaluate the
840 potentialities and limitations of the proposed methodology, a complex case study was
841 chosen; the Roman bridge over the Adaja River, in Castile and León, Spain. Result of the
842 application of the proposed methodology, the developed computational model was able
843 to capture six of the seven modes detected during the ambient vibration tests. These
844 modes shown an average relative error in frequencies of about 2.22% and an average
845 MAC value of 0.91, corroborating the robustness of the proposed method. Finally, the
846 performance of the structure against vertical loadings is evaluated and contrasted with a
847 numerical model created by means of the data obtained in the literature (no experimental
848 data). This comparison highlights the relevance of this methodology, obtaining a
849 discrepancy of 25% in terms of safety factor. Complementary to this evaluation, and
850 taking into consideration the advantages of the finite element method, several numerical
851 simulations were carried out with the aim of evaluating the performance of the bridge in
852 case of continuing the material loses. In all the simulations the results suggest that the
853 bridge has an excellent bearing capacity, being safe in the medium-long term to the
854 material loses that is suffering.
855
856 Futures improvement of the methdodology will be focused on several aspects: i) the use
857 of automatic updating strategies such as those proposed by [25, 27, 32] based on genetic
858 and deterministic approaches; ii) further validation of the multichannel analysis of surface
859 waves tests as a potential approach for the analysis of the infill materials and iii) the study
860 of the possible relation between the data provided by the multichannel analysis of surface
861 waves tests and the non-linear properties of the infill materials.
862
863

Acknowledgments

This work was financed by ERDF funds through the V SUDOE INTERREG program within the framework of the HeritageCARE project, Ref. SOE1/P5/P0258 and the research project Patrimonio 5.0 funded by Junta of Castilla y León, Ref. SA075P17. First author would like to thank the University of Salamanca for the program for human resources "Programa II: Contratos Postdoctorales". Authors also wish to thanks to the council of Avila for their support in gathering the historical documentation of the bridge.

References

[1] I. Olofsson, L. Elfgren, B. Bell, B. Paulsson, E. Niederleithinger, J. Sandager Jensen, G. Feltrin, B. Täljsten, C. Cremona, R. Kiviluoma, Assessment of European railway bridges for future traffic demands and longer lives–EC project "Sustainable Bridges", Structure and Infrastructure Engineering 1(2) (2005) 93-100. DOI: 10.1080/15732470412331289396

[2] B. Conde, P. Eguía, G.E. Stavroulakis, E. Granada, Parameter identification for damaged condition investigation on masonry arch bridges using a Bayesian approach, Engineering Structures 172 (2018) 275-284. DOI: 10.1016/j.engstruct.2018.06.040

[3] C. Modena, G. Tecchio, C. Pellegrino, F. da Porto, M. Donà, P. Zampieri, M.A. Zanini, Reinforced concrete and masonry arch bridges in seismic areas: typical deficiencies and retrofitting strategies, Structure and Infrastructure Engineering 11(4) (2015) 415-442. DOI: 10.1080/15732479.2014.951859

[4] V. Sarhosis, S. De Santis, G. de Felice, A review of experimental investigations and assessment methods for masonry arch bridges, Structure and Infrastructure Engineering 12(11) (2016) 1439-1464. DOI: 10.1080/15732479.2015.1136655

[5] P. Zampieri, M.A. Zanini, F. Faleschini, L. Hofer, C. Pellegrino, Failure analysis of masonry arch bridges subject to local pier scour, Engineering failure analysis 79 (2017) 371-384. DOI: 10.1016/j.engfailanal.2017.05.028

[6] A. Arêde, C. Costa, A.T. Gomes, J.E. Menezes, R. Silva, M. Morais, R. Gonçalves, Experimental characterization of the mechanical behaviour of components and materials of stone masonry railway bridges, Construction and Building Materials 153 (2017) 663-681. DOI: 10.1016/j.conbuildmat.2017.07.069

[7] A.C. Aydin, S.G. Özkaya, The finite element analysis of collapse loads of single-spanned historic masonry arch bridges (Ordu, Sarpdere Bridge), Engineering Failure Analysis 84 (2018) 131-138. DOI: 10.1016/j.engfailanal.2017.11.002

[8] B. Conde, L.F. Ramos, D.V. Oliveira, B. Riveiro, M. Solla, Structural assessment of masonry arch bridges by combination of non-destructive testing techniques and three-dimensional numerical modelling: Application to Vilanova bridge, Engineering Structures 148 (2017) 621-638. DOI: 10.1016/j.engstruct.2017.07.011

[9] G. Milani, P.B. Lourenço, 3D non-linear behavior of masonry arch bridges, Computers & Structures 110 (2012) 133-150. DOI: 10.1016/j.compstruc.2012.07.008

[10] E. Bertolesi, G. Milani, F.D. Lopane, M. Acito, Augustus Bridge in Narni (Italy): Seismic Vulnerability Assessment of the Still Standing Part, Possible Causes of Collapse, and Importance of the Roman Concrete Infill in the Seismic-Resistant Behavior, International Journal of Architectural Heritage 11(5) (2017) 717-746. DOI: 10.1080/15583058.2017.1300712

[11] S. Degli Abbati, A.M. D'Altri, D. Ottonelli, G. Castellazzi, S. Cattari, S. de Miranda, S. Lagomarsino, Seismic assessment of interacting structural units in complex historic masonry constructions by nonlinear static analyses, Computers & Structures 213 (2019) 51-71. DOI: 10.1016/j.compstruc.2018.12.001

[12] Á. Bautista-De Castro, L.J. Sánchez-Aparicio, L.F. Ramos, J. Sena-Cruz, D. González-Aguilera, Integrating geomatic approaches, Operational Modal Analysis, advanced numerical and updating methods to evaluate the current safety conditions of the historical Bôco Bridge, Construction and Building Materials 158 (2018) 961-984. DOI: 10.1016/j.conbuildmat.2017.10.084
[13] J.P.C. Pérez, J.J. de Sanjosé Blasco, A.D. Atkinson, L.M. del Río Pérez, Assessment of the Structural Integrity of the Roman Bridge of Alcántara (Spain) Using TLS and GPR, Remote Sensing 10(3) (2018) 387. DOI: 10.3390/rs10030387
[14] V.N. Moreira, J.C. Matos, D.V. Oliveira, Probabilistic-based assessment of a masonry arch bridge considering inferential procedures, Engineering Structures 134 (2017) 61-73. DOI: 10.1016/j.engstruct.2016.11.067
[15] M.E. Stavroulaki, B. Riveiro, G.A. Drosopoulos, M. Solla, P. Koutsianitis, G.E. Stavroulakis, Modelling and strength evaluation of masonry bridges using terrestrial photogrammetry and finite elements, Advances in Engineering Software 101 (2016) 136-148. DOI: 10.1016/j.advengsoft.2015.12.007
[16] C. Pepi, M. Gioffrè, G. Comanducci, N. Cavalagli, A. Bonaca, F. Ubertini, Dynamic characterization of a severely damaged historic masonry bridge, Procedia engineering 199 (2017) 3398-3403. DOI: 10.1016/j.proeng.2017.09.579
[17] B. Riveiro, J. Caamaño, P. Arias, E. Sanz, Photogrammetric 3D modelling and mechanical analysis of masonry arches: An approach based on a discontinuous model of voussoirs, Automation in Construction 20(4) (2011) 380-388. DOI: 10.1016/j.autcon.2010.11.008
[18] B. Riveiro, B. Conde-Carnero, P. Arias-Sánchez, Laser Scanning for the Evaluation of Historic Structures, Civil and Environmental Engineering: Concepts, Methodologies, Tools, and Applications, IGI Global2016, pp. 807-835. DOI: 10.1016/j.autcon.2010.11.008
[19] B. Conde, L. Díaz-Vilariño, S. Lagüela, P. Arias, Structural analysis of Monforte de Lemos masonry arch bridge considering the influence of the geometry of the arches and fill material on the collapse load estimation, Construction and Building Materials 120 (2016) 630-642. DOI: 10.1016/j.conbuildmat.2016.05.107
[20] I. Lubowiecka, P. Arias, B. Riveiro, M. Solla, Multidisciplinary approach to the assessment of historic structures based on the case of a masonry bridge in Galicia (Spain), Computers & Structures 89(17) (2011) 1615-1627. DOI: 10.1016/j.compstruc.2011.04.016
[21] B. Riveiro, P. Morer, P. Arias, I. de Arteaga, Terrestrial laser scanning and limit analysis of masonry arch bridges, Construction and Building Materials 25(4) (2011) 1726-1735. DOI: 10.1016/j.conbuildmat.2010.11.094
[22] M. Korumaz, M. Betti, A. Conti, G. Tucci, G. Bartoli, V. Bonora, A.G. Korumaz, L. Fiorini, An integrated Terrestrial Laser Scanner (TLS), Deviation Analysis (DA) and Finite Element (FE) approach for health assessment of historical structures. A minaret case study, Engineering Structures 153 (2017) 224-238. DOI: 10.1016/j.engstruct.2017.10.026
[23] A.M. D'Altri, G. Milani, S. de Miranda, G. Castellazzi, V. Sarhosis, Stability analysis of leaning historic masonry structures, Automation in Construction 92 (2018) 199-213. DOI: 10.1016/j.autcon.2018.04.003
[24] S.G. Barsanti, G. Guidi, A geometric processing workflow for transforming reality-based 3D models in volumetric meshes suitable for FEA, The International Archives of Photogrammetry, Remote Sensing and Spatial Information Sciences 42 (2017) 331. DOI: 10.5194/isprs-archives-XLII-2-W3-331-2017, 2017

[25] L.J. Sánchez-Aparicio, B. Riveiro, D. Gonzalez-Aguilera, L.F. Ramos, The combination of geomatic approaches and operational modal analysis to improve calibration of finite element models: A case of study in Saint Torcato Church (Guimarães, Portugal), Construction and Building Materials 70 (2014) 118-129. DOI: 10.1016/j.conbuildmat.2014.07.106

[26] G. Castellazzi, A.M. Altri, G. Bitelli, I. Selvaggi, A. Lambertini, From Laser Scanning to Finite Element Analysis of Complex Buildings by Using a Semi-Automatic Procedure, Sensors 15(8) (2015) 18360-18380. DOI: 10.3390/s150818360

[27] E. Bassoli, L. Vincenzi, A.M. D'Altri, S. de Miranda, M. Forghieri, G. Castellazzi, Ambient vibration-based finite element model updating of an earthquake-damaged masonry tower, Structural Control and Health Monitoring 25(5) (2018) e2150. DOI: 10.1002/stc.2150

[28] R. Aguilar, M.F. Noel, L.F. Ramos, Integration of reverse engineering and non-linear numerical analysis for the seismic assessment of historical adobe buildings, Automation in Construction 98 (2019) 1-15. DOI: 10.1016/j.autcon.2018.11.010

[29] M. Solla, R. Asorey-Cacheda, X. Núñez-Nieto, B. Conde-Carnero, Evaluation of historical bridges through recreation of GPR models with the FDTD algorithm, NDT & E International 77 (2016) 19-27. DOI: 10.1016/j.ndteint.2015.09.003

[30] A. Arce, L.F. Ramos, F.M. Fernandes, L.J. Sánchez-Aparicio, P.B. Lourenço, Integrated structural safety analysis of San Francisco Master Gate in the Fortress of Almeida, International Journal of Architectural Heritage 12 (2017) 761-778. DOI: 10.1080/15583058.2017.1370507

[31] C. Costa, A. Arêde, António, A. Costa, Aníbal, Mechanical characterization of the constituent materials of stone arch bridges, 9th International Masonry Conference, Guimaraes, Portugal, 2014.

[32] C. Costa, D. Ribeiro, P. Jorge, R. Silva, A. Arêde, R. Calçada, Calibration of the numerical model of a stone masonry railway bridge based on experimentally identified modal parameters, Engineering Structures 123 (2016) 354-371. DOI: 10.1016/j.engstruct.2016.05.044

[33] K. Charter, Principles for conservation and restoration of built heritage, Marsilio, Venice, http://smartheritage.com/wp-content/uploads/2015/03/KRAKOV-CHARTER-2000.pdf (Accessed 06/04/2016 2019).

[34] I. Lubowiecka, J. Armesto, P. Arias, H. Lorenzo, Historic bridge modelling using laser scanning, ground penetrating radar and finite element methods in the context of structural dynamics, Engineering Structures 31(11) (2009) 2667-2676. DOI: 10.1016/j.engstruct.2009.06.018

[35] A. Blanco Freijeiro, Informes académicos. Puente romano sobre el río Adaja, en Ávila, Boletín de la Real Academia de la Historia (1985) 144-145.

[36] M.C. Tomás, La manipulación del patrimonio cultural: la Fábrica de Harinas de Ávila, Política y sociedad (27) (1998) 89-116.

[37] C. León, F.L.M. Jesus, Memoria valorada para la actuación urgente en el Puente romano sobre el Río Adaja, Obras municipales 80/6, Avila, 1995, p. 54.

[38] HeritageCARE, Survey of construction systems, type of damages and deterioration processes within the SUDOE territory, HeritageCARE project, http://heritagecare.eu/wp-content/uploads/2017/09/HeritageCARE-Report-1.1.pdf (Accessed 06/04/2016 2019).

[39] J. Garcia-Talegon, A.C. Iñigo, S. Vicente-Tavera, E. Molina-Ballesteros, Heritage Stone 5. Silicified Granites (Bleeding Stone and Ochre Granite) as Global Heritage Stone Resources from Ávila, Central Spain, Geoscience Canada 43(1) (2016) 53-62. DOI: 10.12789/geocanj.2016.43.087

[40] L.J. Sánchez-Aparicio, S. Del Pozo, L.F. Ramos, A. Arce, F.M. Fernandes, Heritage site preservation with combined radiometric and geometric analysis of TLS data, Automation in Construction 85 (Supplement C) (2018) 24-39. DOI: 10.1016/j.autcon.2017.09.023
[41] A. Bienert, H.-G. Maas, Methods for the automatic geometric registration of terrestrial laser scanner point clouds in forest stands, ISPRS International Archives of Photogrammetry Remote Sensing and Spatial Information Sciences, Paris, France ,2009 93-98. DOI: 10.1.1.409.8724
[42] N.J. Carino, The impact-echo method: an overview, ASCE World Structural Engineering Conference (2001), pp. 1-18.
[43] L. Miranda, L. Cantini, J. Guedes, A. Costa, Assessment of mechanical properties of full-scale masonry panels through sonic methods. Comparison with mechanical destructive tests, Structural Control and Health Monitoring 23(3) (2016) 503-516. DOI: 10.1002/stc.1783
[44] G. Grandjean, I. Cousin, M. Seger, J. Thiesson, S. Lambot, B. Van Wesemael, A. Stevens, K. Samyn, A. Bitri, S. Bernardi, From geophysical parameters to soil characteristics, DIGISOIL project, https://pdfs.semanticscholar.org/832b/3bef86f6889d7bd8dfa268f5bd7d23365bce.pdf?_ga=2.47695463.1384578154.1554894584-921443786.1548157246 (Accessed 06/04/2016 2019).
[45] C.B. Park, R.D. Miller, J. Xia, Multichannel analysis of surface waves, Geophysics 64(3) (1999) 800-808. DOI: 10.1190/1.1444590
[46] L. Knopoff, Observation and inversion of surface-wave dispersion, Tectonophysics 13(1-4) (1972) 497-519. DOI: 10.1016/0040-1951(72)90035-2
[47] G. Frunzio, M. Monaco, A. Gesualdo, 3D FEM analysis of a roman arch bridge, Proceeding of Historical constructions, Guimaraes, Portugal, 2001 591-598.
[48] L. Pelà, A. Aprile, A. Benedetti, Comparison of seismic assessment procedures for masonry arch bridges, Construction and Building Materials 38 (2013) 381-394. DOI: 10.1016/j.conbuildmat.2012.08.046
[49] R. Brincker, L. Zhang, P. Andersen, Modal identification from ambient responses using frequency domain decomposition, Proceedings of SPIE- The International Society for Optical Engineering , San Antonio, Texas, 2000.
[50] J. Wang, D. Gu, Z. Yu, C. Tan, L. Zhou, A framework for 3D model reconstruction in reverse engineering, Computers & Industrial Engineering 63(4) (2012) 1189-1200. DOI: 10.1016/j.cie.2012.07.009
[51] T. DIANA, https://dianafea.com/, 2019. (Accessed 06/04/2016 2019).
[52] European Committee for Standardization, Eurocode 6: Design of masonry structures—Part 1-1: General rules for reinforced and unreinforced masonry structures, Comité Européen de Normalisation, Brussels, Belgium (2005).
[53] J. García Talegón, A.C. Iñigo, M. Vicente Hernández, M. Vargas, J.L. Pérez Rodríguez, E. Molina Ballesteros, Granitos empleados en Ávila-España. I. Composición química de las distintas variedades, (1994). DOI: 10.3989/mc.1994.v44.i233.594
[54] European Committee for Standardization, EN 1992-1-1 Eurocode 2: Design of concrete structures - Part 1-1: General ruels and rules for buildingsComité Européen de Normalisation, Brussels, Belgium (2005).
[55] R.J. Allemang, The modal assurance criterion–twenty years of use and abuse, Sound and vibration 37(8) (2003) 14-23. DOI: 10.1.1.582.30
[56] M. Tomaževič, Earthquake-resistant design of masonry buildings, first ed., Imperial College Press, London, 1999. ISBN: 978-1-84816-083-5

[57] P. Lourenço, Recent advances in masonry structures: micromodelling and homogeneization, in U. Galvanetto, MH Ferri Aliabadi (Eds.), Multiscale modeling in solid mechanics: computational approaches, Imperial College Press, London, 2009, pp. 251-294. ISBN: 184816307X

[58] G. Toniolo, M. di Prisco, Reinforced concrete design to Eurocode 2, first ed., Springer, London, 2017. ISBN: 978-3-319-52033-9

[59] Ministerio delle infrastructure e dei trasporti, Norme tecniche per le costruzioni, Decreto Ministeriale del 14, 2008. http://www.cslp.it/cslp/index.php?option=com_content&task=view&id=66&Itemid=1 (Accessed 06/04/2016 2019).